A unifying model for hyporheic oxygen mass transfer under a wide range of near-bed hydrodynamic conditions

Chieh-Ying Chen[1], Dimitrios K. Fytanidis[1], and Marcelo H García[2]

[1]University of Illinois at Urbana-Champaign
[2]University of Illinois at Urbana Champaign

August 12, 2023

Abstract

Existing models for estimating hyporheic oxygen mass transfer often require numerous parameters related to flow, bed, and channel characteristics, which are frequently unavailable. We performed a meta-analysis on existing dataset, enhanced with high Reynolds number cases from a validated Computational Fluid Dynamics model, to identify key parameters influencing effective diffusivity at the sediment water interface. We applied multiple linear regression to generate empirical models for predicting eddy diffusivity. To simplify this, we developed two single-parameter models using either a roughness or permeability-based Reynolds number. These models were validated against existing models and literature data. The model using roughness Reynolds number is easy to use and can provide an estimate of the oxygen transfer coefficient, particularly in scenarios where detailed bed characteristics such as permeability might not be readily available.

A unifying model for hyporheic oxygen mass transfer under a wide range of near-bed hydrodynamic conditions

Chieh-Ying Chen[1], Dimitrios K. Fytanidis[2], and Marcelo H. Garcia[3,4]

[1]Graduate Student, Ven Te Chow Hydrosystems Laboratory, Department of Civil and Environmental Engineering, University of Illinois at Urbana-Champaign, 205 North Mathews Ave., Urbana, IL 61801. Email: cyc2@illinois.edu
[2]Adjunct Research Assistant Professor, Ven Te Chow Hydrosystems Laboratory, Department of Civil and Environmental Engineering, University of Illinois at Urbana-Champaign, 205 North Mathews Ave., Urbana, IL 61801. Email: fytanid2@illinois.edu
[3]M.T. Geoffrey Yeh Endowed Chair and Director, Ven Te Chow Hydrosystems Laboratory, Department of Civil and Environmental Engineering, University of Illinois at Urbana-Champaign, 205 North Mathews Ave., Urbana, IL 61801. Email: mhgarcia@illinois.edu
[4]Centro Internacional de Estudios de Grandes Ros, Facultad de Ingeniera y Ciencias Hdricas, Universidad Nacional del Litoral, Santa Fe City, Santa Fe CP 3000, Argentina.

Key Points:

- We performed reanalysis of flume/field data combined with numerical results to develop models for the oxygen hyporheic mass exchange rate.
- We used a validated numerical model to expand the available dataset of hyporheic oxygen mass exchange under various bed and flow conditions.
- We proposed unifying single-parameter models for the estimation of hyporheic oxygen mass coefficient in open-channel flows.

Corresponding author: Chieh-Ying Chen, `cyc2@illinois.edu`

Abstract

Existing models for estimating hyporheic oxygen mass transfer often require numerous parameters related to flow, bed, and channel characteristics, which are frequently unavailable. We performed a meta-analysis on existing dataset, enhanced with high Reynolds number cases from a validated Computational Fluid Dynamics model, to identify key parameters influencing effective diffusivity at the sediment water interface. We applied multiple linear regression to generate empirical models for predicting eddy diffusivity. To simplify this, we developed two single-parameter models using either a roughness or permeability-based Reynolds number. These models were validated against existing models and literature data. The model using roughness Reynolds number is easy to use and can provide an estimate of the oxygen transfer coefficient, particularly in scenarios where detailed bed characteristics such as permeability might not be readily available.

Plain Language Summary

Current methods for estimating how oxygen is transferred in the sediment-water interface of rivers often require a lot of information about things like the flow and the riverbed characteristics. Unfortunately, this information is often not easy to get. We did a study looking at existing data from flume experiments and the field and added new data from a verified computational model. We wanted to identify which factors are most important in determining how much oxygen moves towards the bed at the sediment-water interface. Using some statistical mathematical tools, we came up with two simple models that only need one piece of information to make predictions. One model considers sediment size, the other looks at riverbed permeability. We validated these models by comparing them to existing methods and data from other studies, and they performed well. The model based on sediment size, which also reflects the roughness of the riverbed, performs best and is the most user-friendly because it does not require information about permeability, which is harder to estimate. This model can provide a reliable estimate of how oxygen moves at the sediment-water interface, particularly when specific details about the riverbed are not available.

1 Introduction

Dissolved oxygen (DO) is a critical component in aquatic ecosystems, impacting nutrient cycling, algae growth, aquatic life maintenance, and pollutant removal in water and sediment (Chapra, 2008). At the sediment-water interface (SWI), sediment oxygen demand (SOD) functions as an oxygen removal flux, transporting dissolved oxygen (DO) from the water to the sediment. This balances the penetration of DO caused by near-bed turbulence with the DO consumed by sediment and benthic chemical processes within the bed (Jørgensen & Revsbech, 1985; Gundersen & Jorgensen, 1990; Mackenthun & Stefan, 1998; Boudreau & Jorgensen, 2001). Accurate modeling of DO dynamics and oxygen mass transfer at the SWI is crucial for understanding nutrient cycling in riverine systems (Waterman et al., 2009; Motta et al., 2010; Waterman et al., 2011; Boano et al., 2014; Waterman et al., 2016).

In smooth-wall hyporheic flows, the oxygen mass transfer coefficient (K_L) is a function of DO diffusivity (D_{eff}) and diffusive layer thickness (δ_{DL}): $K_L = D_{eff}/\delta_{DL}$ at the SWI. K_L is affected by flow shear velocity (u_*), Reynolds number, bed roughness, and the momentum exchange due to hyporheic flow. O'Connor et al. (2009) summarized data for K_L from the literature collected over hydrodynamically smooth beds (Shaw & Hanratty, 1977; Dade, 1993; Steinberger & Hondzo, 1999; Hondzo et al., 2005; Arega & Lee, 2005; O'Connor & Hondzo, 2008) and expressed the dimensionless mass transfer coefficient (K_{L+}) as a function of a temperature-dependent Schmidt number (S_c): $K_{L+} = K_L/u_* = \alpha S_c^{\beta}$, with ranges for α and β being 0.052 to 0.164 and -0.704 to -0.67, respectively. K_{L+} has Reynolds number dependence at low and moderate Reynolds number flows and reaches a self-similar plateau value for large enough Reynolds numbers (Shaw & Hanratty, 1977; Steinberger & Hondzo, 1999).

High roughness height, bed permeability (Perry et al., 1969; Raupach et al., 1991; Jiménez, 2004; Wu et al., 2019), and bed forms (Elliott & Brooks, 1997; Marion et al., 2002; Packman et al., 2004; Tonina & Buffington, 2007) can also enhance hyporheic momentum exchange and thus the mass transfer by increasing the shear stress at the SWI. Han et al. (2018) summarized K_{L+} values from experimental studies over rough beds and found that rough bed K_{L+} values can be up to two orders of magnitude higher than those over smooth beds (Nagaoka & Ohgaki, 1990; Inoue & Nakamura, 2011; Han et al., 2018). OConnor (1984) studied the transfer coefficient for open-channel flows with smooth and rough beds and proposed an analytical equation for the transitional regime. δ_{DL} values are difficult to be estimated for the case of rough wall. Thus, different length scales may be used as flow characteristic length scales at the SWI of rough walls. Nagaoka and Ohgaki (1990) adopted a pore scale restricted mixing length $B = \frac{2\phi^2}{3(1-\phi)}D$ for the estimation of D_{eff} at the SWI. Manes et al. (2012) and Voermans et al. (2017) proposed flow length scales associated with characteristic turbulent eddy size across the SWI (δ_p^*) and the depth of turbulent shear penetration in the bed (δ_p) respectively. Another relevant length scale is the vertical location of the inflection point in the mean velocity profile δ (where $\frac{dU^2}{dz^2} = 0$ and $\frac{d<\overline{U}>}{dz}$ is maximum) which also corresponds to the position of the SWI defined with respect to the top of the sediments (Voermans et al., 2017).

Experimental studies using Particle Image Velocimetry (PIV) (Goharzadeh et al., 2005; Manes et al., 2009; Voermans et al., 2017; Kim et al., 2018; Wu et al., 2019; Kim et al., 2020) have examined the effect of Reynolds number, bed roughness, and bed permeability on eddy viscosity and diffusivity at the SWI. The flow structure at the SWI and inside the bed has been studied numerically using Direct Numerical Simulation (DNS) (Breugem & Boersma, 2005; Breugem et al., 2006; Kuwata & Suga, 2019) and Large Eddy Simulation (LES) (Stoesser et al., 2007; Han et al., 2018; He et al., 2019; Lian et al., 2019, 2021) models. Different scaling parameters for modeling the effective oxygen diffusivity have been proposed by these studies, including bulk Reynolds number (Packman et al., 2004), roughness Reynolds number, and permeability-based Reynolds and Peclet numbers (Grant et al., 2012; Voermans et al., 2017, 2018b). O'Connor and Harvey (2008) summarized the different modes of hyporheic exchange (molecular diffusion, bioturbation, advection, shear, bed mobility, and turbulence) and developed a scaling relationship for the effective diffusion coefficient (D_{eff}) based on a roughness Reynolds number ($Re_* = k_s u_*/\nu$, where u_* is the shear velocity and k_s is roughness height) with a permeability-based Peclet number ($Pe_k = \sqrt{K}u_*/D_m$, K is bed permeability and D_m is the molecular diffusivity). Grant et al. (2012) used both inner and outer scales combined with multiple linear regression (MLR) over an extensive dataset from the literature and found that D_{eff}/D_m has a strong relationship with permeability Reynolds number ($Re_k = \sqrt{K}u_*/\nu$), a Reynolds number defined using the bed thickness ($Re_{H_b} = H_b u_*/\nu$), and porosity ϕ. Voermans et al. (2017, 2018b) conducted a series of experiments across different ranges of permeability, showing the dependencies of D_{eff}/D_m, δ_p and δ_{p*} on Re_k. They also identified a critical Re_k value (Re_k ~1-2) above which turbulence exchange effects dominate over dispersion at the SWI. Finally, the Re_k and Re_* values for these analyses range between $0.01 - 10$ and $1 - 10^4$, respectively.

However, in practice, an ***a priori*** estimation or measurement of permeability can be challenging. Additional experimental tests, e.g., Darcy's permeability measurement (Darcy, 1856), or correlations and analytical expressions between different bed parameters, e.g., the KozenyCarman model (Kozeny, 1927; Bear, 1972), are required for permeability estimation.

In our work, we focused on extending the analysis previously done for the scaling and modeling of effective diffusivity, estimating oxygen mass transfer coefficient, and developing new simple relationships for the estimation of these parameters in practice. We used a computationally efficient method, IDDES (Improved Delayed Detached Eddy Simulations), to extend the range of previously reported Re_k and Re_* in ranges that measurements are not available to date. The numerical results were compared and validated against data from the literature. We also performed a reanalysis and MLR using data from the literature combined with our numerical results to reexamine the relationships between D_{eff}/D_m and inner and outer-/bulk parameters of the bed and the flow. Finally, novel unifying single-parameter models for the prediction of oxygen mass transfer coefficient using roughness or permeability scales were proposed, based on Re_k and Re_*. The proposed models can accurately predict data from field and laboratory conditions from the literature.

2 Definitions

The vertical hyporheic oxygen exchange flux ($J_{S_{O_2}}$) at the SWI is shown in Figure 1 along with the definitions of the primary parameters influencing it. These parameters include the bulk and near-bed hydrodynamics (U_b, u_*, k_s, H_w) as well as the SWI and porous sediment bed characteristics (K, ϕ, H_b). The total/effective mass flux comprises molecular ($J^{MD}_{S_{O_2}}$), dispersive ($J^{DIS}_{S_{O_2}}$), and turbulent ($J^{T}_{S_{O_2}}$) fluxes, which can be expressed as (Voermans et al., 2018b):

$$J_{S_{O_2}} = J^{MD}_{S_{O_2}} + J^{DIS}_{S_{O_2}} + J^{T}_{S_{O_2}} = -D_m \frac{d\phi < C >}{dz} + \phi < \tilde{w}\tilde{C} > + \phi < \overline{w'C'} > \qquad (1)$$

The quantities mentioned above utilize Reynolds and spatial decompositions: $\psi = \overline{\psi} + \psi'$ and $\overline{\psi} = < \overline{\psi} > + \tilde{\psi}$, in which the variable ψ is represented by overbarred, primed, bracketed, and tilded quantities. These indicate the time-averaged, time-fluctuating, spatially-averaged, and spatial-fluctuating quantities, respectively (Lopez & Garcia, 1997; Nikora et al., 2007; Voermans et al., 2018b).

In this study, we performed IDDES simulations on theoretical cases, employing surrogate beds composed of closely packed, monodisperse spheres, as in previous research examining hyporheic mass exchange (Stoesser et al., 2007; Manes et al., 2009; Wu et al., 2019) (Figures 1a and b). Figure 1b illustrates typical normalized streamwise velocity (u_x) by shear velocity (u_*), while the average velocity profile is depicted in Figure 1c. The inflection point (δ) (Figure 1d) in the streamwise velocity profile signifies the extrusion of bed-penetrating eddies and the virtual "interface" of the bed (Manes et al., 2012; Voermans et al., 2018b). Figure 1c shows typical shear stresses as they are computed by the deployed numerical method: $\tau_{total} = \tau_\nu + \tau_{RS} + \tau_{form}$ (Nikora et al., 2007), where τ_{total} is estimated as the integral of viscous and drag forces over the top hemispheres and follows a linear profile until $\tau_{total} = 0$ at $z = H_w$ as $\tau_{total} = \tau_{bed}(1 - z/H_w)$ ($\tau_{bed} = \tau_{total}(z_{bed}) = \int_A F_{viscous} + F_{pressure} dA$, where A is the area of the bed above z=0), $\tau_\nu = \mu d < \overline{u} > /dz$ is the viscous stresses, τ_{RS} is the sum of resolved and modeled Reynolds stresses, and τ_{form} is the form-induced stresses.

This length scale (δ) is preferred over penetration length scale (δ_p) and total height (δ_{p*}) due to its independence from the need for endoscopic measurement techniques (Blois et al., 2014) or refractive index matching (Voermans et al., 2017), even though porous bed permeability still influences δ. Later in the paper, we capitalize on the benefits of δ to create an easy-to-use predictor for hyporheic mass exchange under a variety of flow and bed conditions.

3 Computational Fluid Dynamics Solver

Using the Detached Eddy Simulation (DES) approach, we expanded our dataset via 3D hydrodynamic simulations of hyporheic boundary layer flows with OpenFOAM. We employed the PIMPLE algorithm for incompressible 3D Navier-Stokes equations and

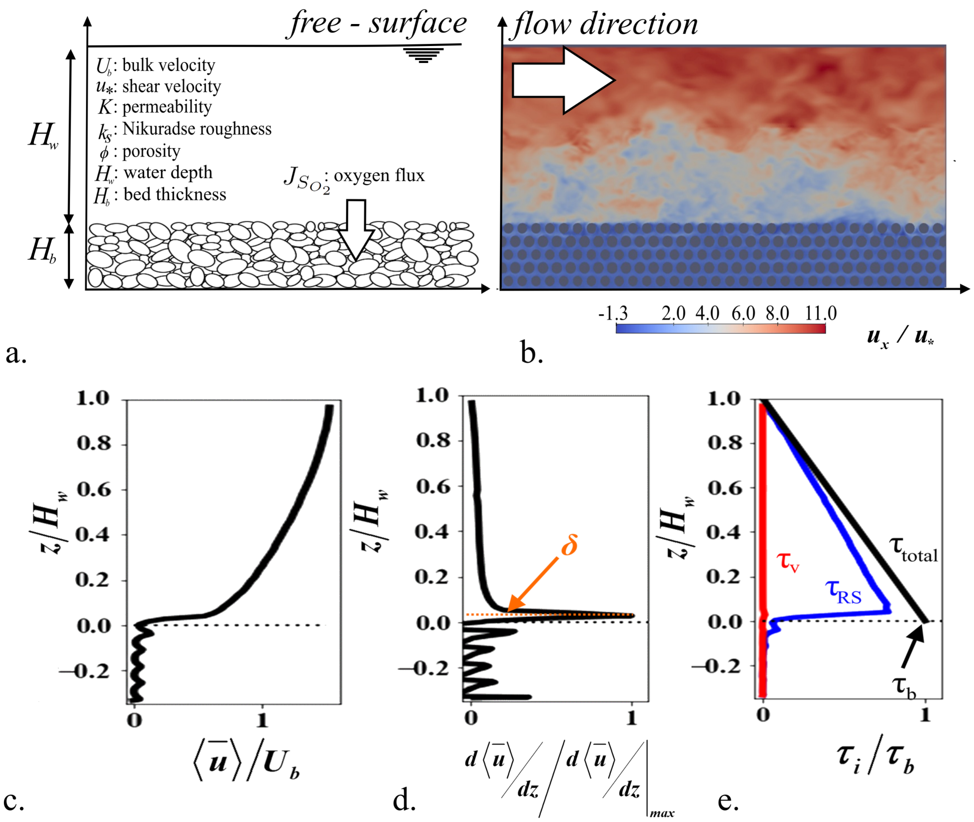

Figure 1. (a) Schematic plot of the problem and definition of quantities, (b) instantaneous u_x/u_* over the surrogate bed, (c) ensembled average velocity profile, (d) normalized ensembled velocity gradient, (e) shear stress distribution.

applied the Spalart-Allmaras Improved Delayed Detached Eddy Simulation (SA-IDDES) for modeling ν_{eff}. The equations of motion were solved assuming that the flows were both incompressible and isothermal. This model was validated using benchmark hyporheic flow cases, compared against Smagorinsky LES model simulations and literature data. We performed detailed analysis to establish result independence considering domain size, boundary conditions, mesh resolutions, and integration time (see supporting information for details - SI1). Figures 2a-d summarize the comparisons of one of the simulations performed herein in dashed lines for the mean velocity (U_x), Reynolds stresses ($\sqrt{\overline{u'w'}}/u_*$) and the variances ($\sigma_u/u_*$ and σ_w/u_*) with measurements performed by Manes et al. (2009) for five-layer low-Re case (Re_k=31.2) and the LES results by Lian et al. (2021) for Re_k=24.2. Table 1 in supporting information - SI2 summarizes all the cases that have been examined in the present study, aiming to expand the existing dataset for high Reynolds number and roughness cases. Also, in Figures 2c and d the similarity relations introduced by Ghisalberti (2009) for a wide range of obstructed shear flows are shown using dashed gray lines. Figures 2e and f show the normalized $\delta u_*/\nu$ thickness as it compares with the corresponding data in Voermans et al. (2018b) as functions of Re_k and Re_*, where $Re_* = k_s u_*/\nu$ with k_s=2.5D (Note that $\delta = \delta_{p*} - \delta_p$). δ is approximately $\sim$0.145$\times$2.5D=0.36D which is reasonably close to the 0.3 value reported by Voermans et al. (2017). Figures 2g and h show the mixing-length ($< L_m >= \sqrt{< \overline{u'w'} > /(dU/dz)^2}$) as functions of Re_k and Re_*. The predictions are reasonably close to those by Voermans et al. (2018b).

4 Hyporheic Mass Exchange Rate and Effective Diffusivity

The effective diffusivity (D_{eff}) can be used to parameterize mass hyporheic exchange under the assumption that the mass transport of oxygen in the sediment bed can be modeled by Ficks second law, which can be expressed for homogeneous porous mediums as (Grant et al., 2012):

$$\frac{d\phi C_{O_2}}{dt} = \frac{d}{dz}\left(\phi D_{eff}\frac{dC_{O_2}}{dz}\right) \tag{2}$$

The oxygen flux at the SWI which is a boundary conditions for the above equation is defined as (O'Connor & Harvey, 2008; O'Connor et al., 2009):

$$J_{S_{O_2}} = -D_{eff}\frac{dC_{O_2}}{dz}|_{z=0} = -(D_m + D_{dis} + D_t)\frac{dC_{O_2}}{dz}|_{z=0} = \frac{D_{eff}}{\delta_{DL}}(C_{w_{O_2}} - C_{s_{O_2}}) \tag{3}$$

In Figure 1a, we defined the oxygen flux ($J_{S_{O_2}}$) which under equilibrium should balance the oxygen consumed within the sediment bed by chemical processes. This mass exchange flux includes the effect of molecular (D_m), dispersive (D_{dis}) and turbulent (D_t) diffusivities (Voermans et al., 2018b). For the case of smooth beds, D_{eff}/δ_{DL} are typically used for the computation of the oxygen flux. In our model we will replace δ_{DL} with inflection point δ, which can be estimated using our numerical results and from empirical equations $\delta_{p*}u_*/\nu = 22Re_k^{1.2}$ and $\delta_p u_*/\nu = 8Re_k^{1.8}$ introduced by Voermans et al. (2018b).

5 Analysis and Results

5.1 Parameterization for D_{eff}

We followed a similar approach as O'Connor and Harvey (2008) and Grant et al. (2012) for parameterizing the effective diffusivity (D_{eff}). Specifically, we used Buckingham's Pi theorem to create dimensionless groupings of the controlling independent variables, as demonstrated in O'Connor and Harvey (2008) and Grant et al. (2012):

$$D_{eff} = f(\nu, D_m, H_w, H_b, U_b, u_*, k_s, K, \phi) \tag{4}$$

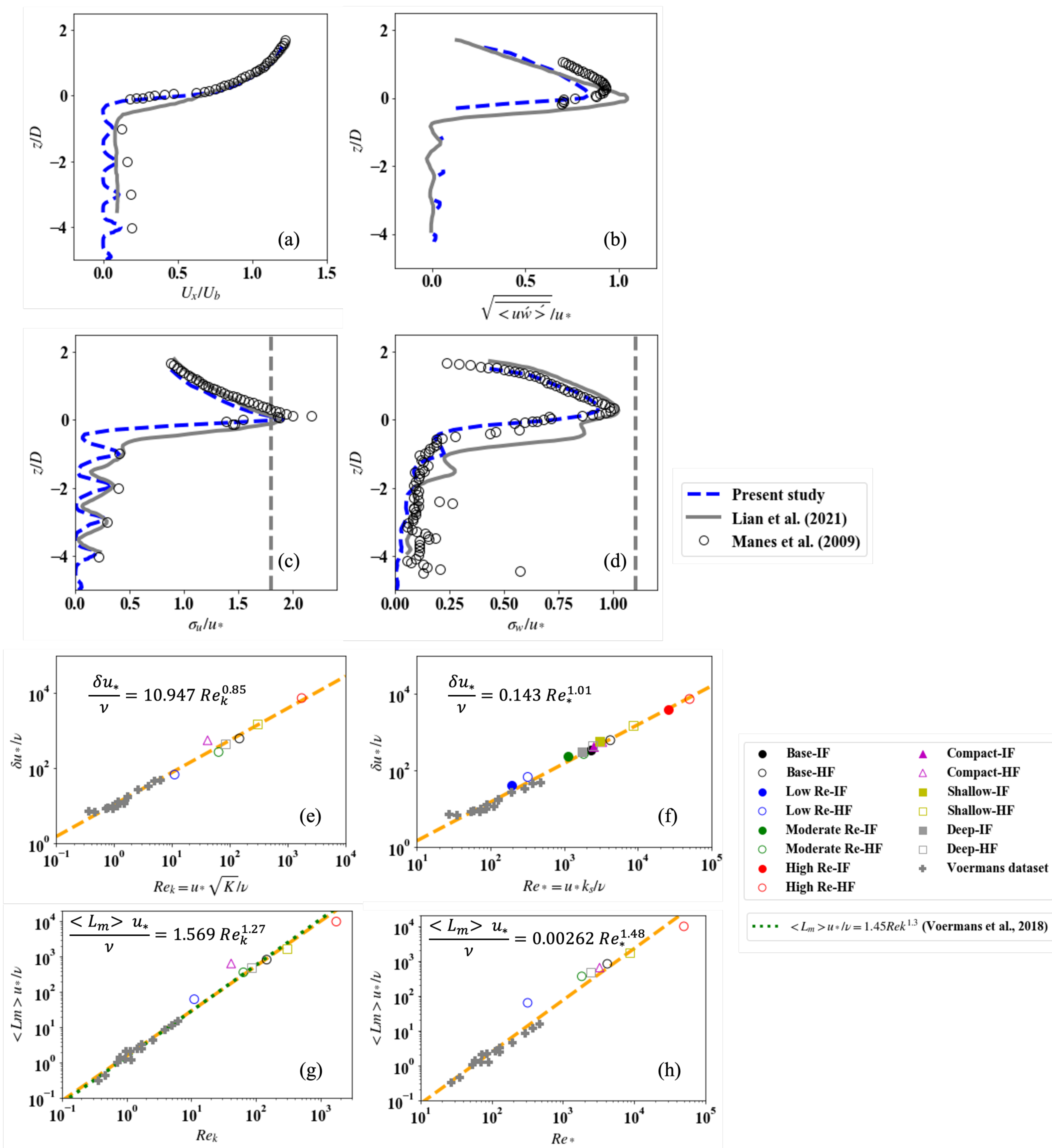

Figure 2. (a), (b), (c) and (d) Typical CFD results and comparison against data from the literature for U_x/U_b, $\sqrt{<\overline{u'w'}>}/u_*$, σ_u/u_* and σ_w/u_*. (e), (f), (g) and (h) fitting relations of length scale δ and mixing length $< L_m >$ with Re_k and Re_*.

In the equation above, there are nine variables (n=9) and two primary dimensions (L, T), m=2. Consequently, a predictive equation for effective diffusivity should have a maximum of seven (n-m=7) non-dimensional groups. For our analysis, we propose that a normalized D_{eff}/D_m can be predicted as a function of the following dimensionless parameters:

$$\frac{D_{eff}}{D_m} = f(Re_{bulk} = \frac{U_b H_w}{\nu}, Re_{Hw} = \frac{u_* H_w}{\nu}, Re_{H_b} = \frac{u_* H_b}{\nu}, Re_* = \frac{u_* k_s}{\nu}, \\ Re_k = \frac{u_* \sqrt{K}}{\nu}, Pe_k = \frac{u_* \sqrt{K}}{D_m}, \phi) \tag{5}$$

Eq.(5) has the potential to account for bulk and near sediment bed hydrodynamic effects (Re_{bulk}, Re_*), SWI exchange (Re_k, Pe_k, ϕ), and flume facility/computational-domain size dependencies (Re_{H_w},Re_{Hb}).

Assuming a power law model (Grant et al., 2012) for modeling the dependence of the equation on the above parameters, we can write:

$$log\frac{D_{eff}}{D_m} = \alpha + \beta logRe_{bulk} + \gamma logRe_{Hw} + \delta logRe_{H_b} + \epsilon logRe_* + \varepsilon logRe_k + \zeta logPe_k + \eta log\phi \tag{6}$$

We used a multiple linear regression (MLR) methodology, following approach used by Grant et al. (2012), to develop a model based on the available data from the literature. This dataset integrates field and flume data from earlier studies (O'Connor & Harvey, 2008; Grant et al., 2012; Voermans et al., 2018b) along with our numerical results. The dataset details are supplied in the supporting information - SI3 and this is the foundation for model development. In testing the possible models, we experimented with 255 different combinations of seven parameters, along with a constant α. The procedure of MLR necessitates that the dependent variable be defined as functions of a group of independent variables, which must not be highly correlated. Thus, it was crucial to initially examine the linearity between dependent and independent variables and then to verify the correlation between chosen independent variables.

Following the approach by Grant et al. (2012), we used the variance inflation factor (VIF) to rule out combinations with high-correlated parameters (Miles, 2014). The VIF is an index indicating the extent to which a given variable is influenced by the variation in other variables. A VIF of 1 signifies no correlation, whereas a higher VIF suggests increased correlation. To strike a balance between model complexity and accuracy, Grant et al. (2012) recommended the use of a combination that excludes any variables with VIF>5 and employs the Akaike information criterion (AIC) as the selection criterion. The AIC estimates the degree of information loss in a model (Akaike, 1974; Sakamoto et al., 1986; Aho et al., 2014). We applied the VIF as a filtering mechanism and the minimum AIC as a selection standard. Table 4 in the supporting information - SI4 summarizes the 5 models with the best fitness to the training data.

Figures 3a, b and c show the fitness of the 3 best performing models. In an effort to develop a simple single-parameter model for all different bed and flow characteristics, D_{eff}/D_m versus every single of the 6 dimensionless numbers considered in our MLR analysis are plotted in Figures 3d-i together with the corresponding R^2 values. It is shown that Re_k and Re_* show the best coefficient of determination, which will be explored as single parameters to develop empirical model for the prediction of the oxygen mass transfer coefficient.

5.2 A unifying model for the hyporheic oxygen mass transfer

In the previous paragraph, we established the best single-parameter models for D_{eff}/D_m based on roughness Reynolds number (Re_*) and permeability Reynolds number (Re_k),

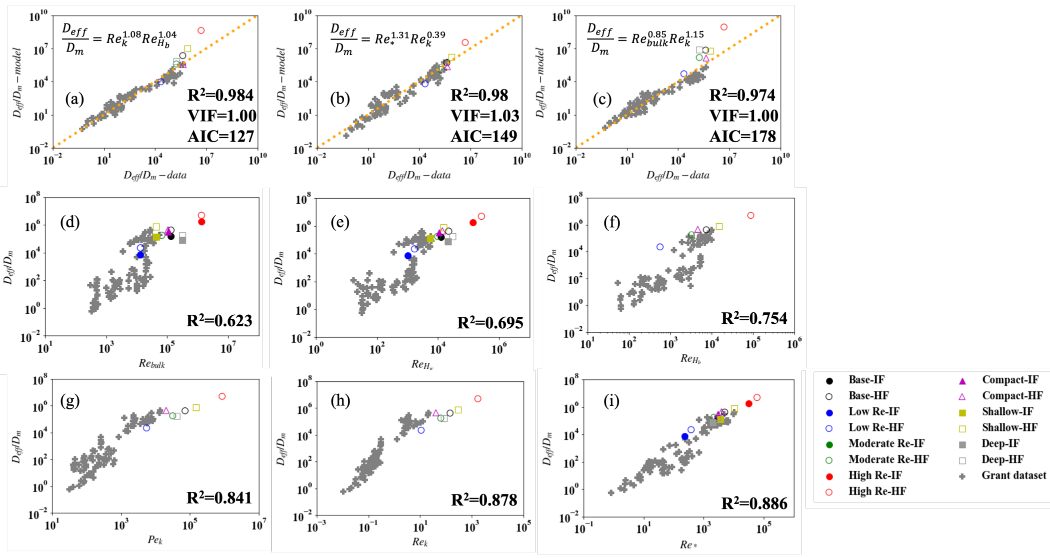

Figure 3. (a), (b), (c) D_{eff}/D_m evaluation of the three best performing MLR models: $Re_k^{1.08} Re_{H_b}^{1.04}$, $Re_*^{1.31} Re_k^{0.39}$, $Re_{bulk}^{0.85} Re_k^{1.15}$. (d), (e), (f), (g), (h), (i) prediction ability by single parameter models: Re_{bulk}, Re_{Hw}, Re_{Hb}, Pe_k, Re_k, Re_*.

given their highest R^2 values. Using these Reynolds numbers, we were able to scale the mass transfer coefficient K_L, forming a new relationship for oxygen mass transfer across diverse roughness and permeability conditions. To address the problem of defining the diffusive layer (δ_{DL}) in rough wall situations, we introduced a unifying transfer coefficient, $\tilde{K_L} = D_{eff}/\delta$ and $\tilde{K_L^+} = \tilde{K_L}/u_*$, applicable to both hydrodynamically smooth and rough cases. This is done using the inflection point δ which can be estimated for all conditions using the equations in Figure 2.

The functions we proposed, represented as $\tilde{K_L^+} = \alpha Re_i^\beta/(Re_i^\beta + \gamma)$, where $Re_i = Re_*$ or Re_k, take inspiration from the sediment entertainment function by Garcia and Parker (1991). These functions describe how $\tilde{K_L^+}$ starts from zero and increases with Re_* and Re_k until it plateaus at higher Re_* and Re_k, aligning with self-similar plateau values proposed by Shaw and Hanratty (1977) and Steinberger and Hondzo (1999).

We used data from O'Connor et al. (2009), Han et al. (2018) and Voermans et al. (2018b), dataset that include smooth to fully rough beds and low to high permeabilities (Steinberger & Hondzo, 1999; O'Connor & Hondzo, 2008; O'Connor et al., 2009; Nagaoka & Ohgaki, 1990; Elliott & Brooks, 1997; Marion et al., 2002; Packman et al., 2004; Tonina & Buffington, 2007; Voermans et al., 2017). All data can be found in Table 5 in the supporting information - SI5. Following regression analysis, we derived two equations, with results displayed in Figures 4a and b:

$$\tilde{K_L^+} = \frac{2.058 Re_*^{0.698}}{Re_*^{0.698} + 412.949} = \frac{2.045 Re_k^{0.729}}{Re_k^{0.729} + 31.973} \tag{7}$$

To validate the accuracy of our model, we tested it against the data used for the MLR. We also used the zonal model by Voermans et al. (2018b) to predict using the same dataset. Note that this dataset is the same one used by Voermans et al. (2018b) for their

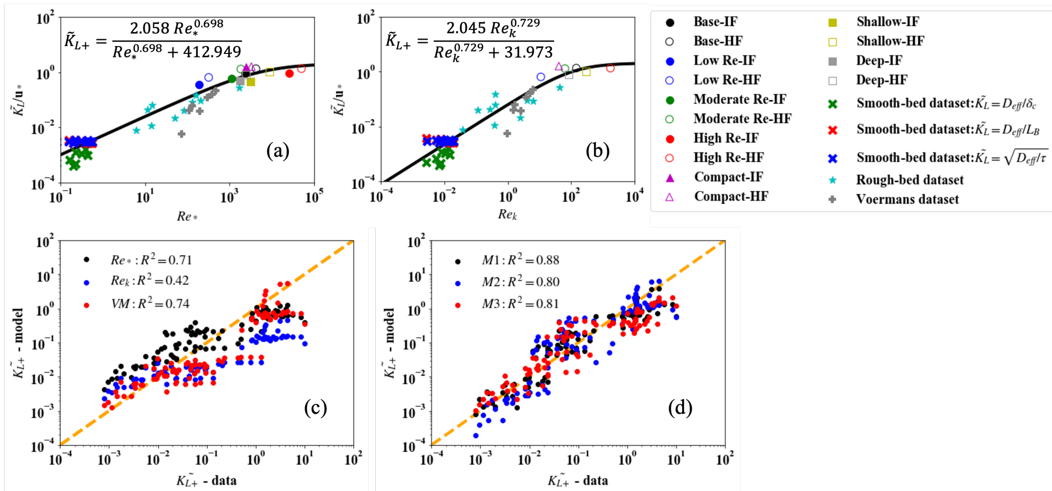

Figure 4. (a), (b) Non-dimensional $\tilde{K}_L^+$ versus Re_* and Re_k. (c) Evaluation of the accuracy of the two proposed models and comparison against zonal model in Voermans et al. (2018b). (d) Evaluation of the three best performing models based on the MLR analysis.

regression. Voermans et al. (2018b)'s zonal model is represented as:

$$\frac{D_{eff}}{D_m} = \begin{cases} 1 & Re_k \leq 0.02 \\ 1.6 Re_k^2 S_c & 0.02 < Re_k < 1 \\ 1.9 Re_k^2 S_c & Re_k \geq 1 \end{cases} \tag{8}$$

The δ values were estimated from closure equations depicted in Figure 2, and the D_m, u_*, k_s, and K values are available for all cases. The performance of the two unified equations proposed in this study is shown in Figure 4c.

The roughness-based Reynolds number model demonstrates a higher R^2 value (0.71) than the permeability-based Reynolds number model (0.42). Voermans et al. (2018b)'s zonal model shows an R^2 value of 0.74, quite close to the Re_*-based model, despite being derived from the validation dataset. Lastly, the three best performing models derived using MLR are also tested against the same dataset (see Figure 4d). As expected, the multi-parameter models proposed here outperform both the single-parameter models and the zonal model by Voermans et al. (2018b), with R^2 values of 0.88, 0.80, and 0.81 respectively.

A big advantage of the unifying model based on Re_* is the fact that it is solely based on the Nikuradse roughness height rather than permeability, which can potentially be more challenging parameter to estimate, i.e. the use of laboratory tests. In fact, even if compared with the prediction by Voermans et al. (2018b)'s zonal model (mean absolute error is 1.05), the MAE is 1.19 for the Re_*-based model while the MAE for the Re_k-based model is 1.66. Finally, the 3 MLR models have typically smaller errors (0.73, 0.97, 0.94 respectively); however, they introduce additional complexity and in some cases, i.e. $D_{eff}/D_m = Re_k^{1.076} Re_{H_b}^{1.038}$, parameters like the thickness of the bed permeable layer (H_b) in Re_{H_b} have more importance when we study the oxygen exchange at a laboratory setting using shallow test flumes or require significant field work to estimate the elevation of any impervious bedrock layer.

6 Applications and Relevant Discussions of the Single-parameter Model

The proposed Re_*-based model outlined earlier requires minimal data inputs. These include some parameter estimations:

- Nikuradse roughness (k_s) can be determined based on characteristic bed diameters as $k_s = \alpha_s D_s$, where D_s could be D_{50} or D_{70}. A comprehensive list of α_s values can be referred to Garcia (2008). For example, $k_s = \alpha_s D_s$=2.5D_{50}.
- Shear velocity (u_*) can be estimated by the friction slope (S_f) data as $u_* = \sqrt{gH_wS_f}$, or referred to nomographs and models for hyporheic friction factors, such as those in Manes et al. (2012) and Voermans et al. (2018a).
- Length scale δ can be calculated by the equations in Figure 2 as $\delta u_*/\nu = 0.143Re_*^{1.01}$ ($\delta \sim$0.143k_s).
- Kinematic viscosity (ν) is a temperature relevant parameter. The ν of water can be estimated using the formula: $\nu = 1.79 \times 10^{-6}/(1 + 0.3368T_c + 0.00021T_c^2)$ with T_c in Celsius.

With the parameters above, $\tilde{K_L}$ can be obtained from Equation (7) by $Re_* = k_s u_*/\nu$ and u_*. The effective oxygen diffusivity can be determined as $D_{eff} = \tilde{K_L}\delta$.

If you have permeability measurements, you can utilize either the Re_k-based model by Re_k in Equation (7) or the zonal model by (Voermans et al., 2018b). The MLR-based models shown in Figure 3 can also estimate D_{eff}/D_m when both k_s and K data are available. If additional data such as the thickness of a permeable layer (H_b) atop an impermeable bottom or other bed thickness restrictions (for instance, in laboratory flume flow cases) are available, you can also use the MLR-derived model based on $Re_{Hb} = u_*H_b/\nu$.

It's crucial to note that the unifying model from Equation (7) can yield D_{eff} values that are smaller than the molecular diffusivity (D_m). This typically occurs in low Reynolds number flows where oxygen mass exchange is primarily driven by molecular diffusion, a less common scenario in open-channel cases. Instances with ratios as low as D_{eff}/D_m=0.6 were reported by Grant et al. (2012) and Voermans et al. (2018b) may have documented cases resulting from tortuosity effects between grains (O'Connor & Harvey, 2008). Voermans et al. (2018b) noted that D_{eff} equals D_m for Re_k less than 0.02 (see Equation (8)). O'Connor and Harvey (2008) suggested a similar criterion of $Re_*Pe_k^{6/5}$ <2000 which leads to $D_{eff} = D_m$ for a tortuosity parameter β=1. The models developed here can be adjusted to consider these criteria by introducing a limiting parameter where D_{eff} is the maximum of the predicted value and D_m (or βD_m if considering tortuosity effects).

7 Conclusion

A meta-analysis of pre-existing datasets, supplemented by high Reynolds number Computational Fluid Dynamics (CFD) results, was conducted to examine the scaling parameters that influence oxygen mass transfer in hyporheic zones. Using this enhanced dataset, multiple linear regression was utilized to create multi-parameter predictive models for effective diffusivity in turbulent hyporheic flows. A novel unifying model was then introduced, aiming to estimate the oxygen mass transfer coefficient using the roughness height rather than bed permeability. This newly developed model underwent validation through comparisons with other models and existing literature data. It is designed to serve as a user-friendly tool that can provide essential data for estimating the oxygen transfer coefficient, particularly in scenarios where detailed bed characteristics might not be readily available.

Data Availability Statement

All numerical results in this manuscript were generated by Openfoam v8 (`https://openfoam.org/version/8/`). Data archiving is underway. The Openfoam setup and numerical results are temporarily uploaded as Supporting Information for review purposes. All the data will be uploaded to Zenodo data repository.

Acknowledgments

The financial support by Metropolitan Water Reclamation District of Greater Chicago (MWRDGC) is gratefully acknowledged. The computational support by National Science Foundation via grant number ACI-1548562 for Extreme Science and Engineering Discovery Environment (XSEDE), now migrated to Advanced Cyberinfrastructure Coordination Ecosystem: Services and Support (ACCESS), is appreciated. This work used XSEDE Stampede2 at the Texas Advanced Computing Center (TACC) through allocation TG-CTS190067 and Frontera at TACC through Pathways allocation CTS22005.

References

Aho, K., Derryberry, D., & Peterson, T. (2014). Model selection for ecologists: the worldviews of aic and bic. *Ecology*, *95*(3), 631–636.

Akaike, H. (1974). A new look at the statistical model identification. *IEEE transactions on automatic control*, *19*(6), 716–723.

Arega, F., & Lee, J. H. (2005). Diffusional mass transfer at sediment–water interface of cylindrical sediment oxygen demand chamber. *Journal of Environmental Engineering*, *131*(5), 755–766.

Bear, J. (1972). *Dynamics of fluids in porous media*. Elsevier, New York.

Blois, G., Best, J. L., Sambrook Smith, G. H., & Hardy, R. J. (2014). Effect of bed permeability and hyporheic flow on turbulent flow over bed forms. *Geophysical Research Letters*, *41*(18), 6435–6442.

Boano, F., Harvey, J. W., Marion, A., Packman, A. I., Revelli, R., Ridolfi, L., & Wörman, A. (2014). Hyporheic flow and transport processes: Mechanisms, models, and biogeochemical implications. *Reviews of Geophysics*, *52*(4), 603–679.

Boudreau, B. P., & Jorgensen, B. B. (2001). *The benthic boundary layer: Transport processes and biogeochemistry*. Oxford University Press.

Breugem, W.-P., Boersma, B., & Uittenbogaard, R. (2006). The influence of wall permeability on turbulent channel flow. *Journal of Fluid Mechanics*, *562*, 35.

Breugem, W.-P., & Boersma, B.-J. (2005). Direct numerical simulations of turbulent flow over a permeable wall using a direct and a continuum approach. *Physics of fluids*, *17*(2), 025103.

Chapra, S. C. (2008). *Surface water-quality modeling*. Waveland press.

Dade, W. B. (1993). Near-bed turbulence and hydrodynamic control of diffusional mass transfer at the sea floor. *Limnology and Oceanography*, *38*(1), 52–69.

Darcy, H. (1856). *Les fontaines publiques de la ville de dijon: exposition et application des principes à suivre et des formules à employer dans les questions de distribution d'eau... un appendice relatif aux fournitures d'eau de plusieurs villes au filtrage des eaux* (Vol. 1). Victor Dalmont, éditeur.

Elliott, A. H., & Brooks, N. H. (1997). Transfer of nonsorbing solutes to a streambed with bed forms: Laboratory experiments. *Water Resources Research*, *33*(1), 137–151.

Engelund, F. (1970). Instability of erodible beds. *Journal of Fluid Mechanics*, *42*(2), 225–244.

Garcia, M. (2008). *Sedimentation engineering: processes, measurements, modeling, and practice. asce manuals and reports on engineering practice no. 110. a.* American Society of Civil Engineers. Reston, VA.

Garcia, M., & Parker, G. (1991). Entrainment of bed sediment into suspension. *Journal of Hydraulic Engineering*, *117*(4), 414–435.

Ghisalberti, M. (2009). Obstructed shear flows: similarities across systems and scales. *Journal of Fluid Mechanics*, *641*, 51–61.

Goharzadeh, A., Khalili, A., & Jørgensen, B. B. (2005). Transition layer thickness at a fluid-porous interface. *Physics of Fluids*, *17*(5), 057102.

Grant, S. B., Stewardson, M. J., & Marusic, I. (2012). Effective diffusivity and mass flux across the sediment-water interface in streams. *Water Resources Research*, *48*(5).

Gundersen, J. K., & Jorgensen, B. B. (1990). Microstructure of diffusive boundary layers and the oxygen uptake of the sea floor. *Nature*, *345*(6276), 604–607.

Han, X., Fang, H., He, G., & Reible, D. (2018). Effects of roughness and permeability on solute transfer at the sediment water interface. *Water research*, *129*, 39–50.

He, G., Han, X., Fang, H., Reible, D., & Huang, L. (2019). Effects of roughness reynolds number on scalar transfer mechanisms at the sediment-water interface. *Water Resources Research*, *55*(8), 6811–6824.

Hondzo, M., Feyaerts, T., Donovan, R., & O'Connor, B. L. (2005). Universal scaling of dissolved oxygen distribution at the sediment-water interface: A power law. *Limnology and oceanography*, *50*(5), 1667–1676.

Inoue, T., & Nakamura, Y. (2011). Effects of hydrodynamic conditions on do transfer at a rough sediment surface. *Journal of Environmental Engineering*, *137*(1), 28–37.

Jiménez, J. (2004). Turbulent flows over rough walls. *Annu. Rev. Fluid Mech.*, *36*, 173–196.

Jørgensen, B. B., & Revsbech, N. P. (1985). Diffusive boundary layers and the oxygen uptake of sediments and detritus. *Limnology and oceanography*, *30*(1), 111–122.

Kim, T., Blois, G., Best, J. L., & Christensen, K. T. (2018). Experimental study of turbulent flow over and within cubically packed walls of spheres: Effects of topography, permeability and wall thickness. *International Journal of Heat and Fluid Flow*, *73*, 16–29.

Kim, T., Blois, G., Best, J. L., & Christensen, K. T. (2020). Experimental evidence of amplitude modulation in permeable-wall turbulence. *Journal of Fluid Mechanics*, *887*.

Kozeny, J. (1927). Uber kapillare leitung der wasser in boden. *Royal Academy of Science, Vienna, Proc. Class I*, *136*, 271–306.

Kuwata, Y., & Suga, K. (2019). Extensive investigation of the influence of wall permeability on turbulence. *International Journal of Heat and Fluid Flow*, *80*, 108465.

Lian, Y. P., Dallmann, J., Sonin, B., Roche, K., Liu, W. K., Packman, A., & Wagner, G. J. (2019). Large eddy simulation of turbulent flow over and through a rough permeable bed. *Computers & Fluids*, *180*, 128–138.

Lian, Y. P., Dallmann, J., Sonin, B., Roche, K. R., Packman, A. I., Liu, W. K., & Wagner, G. J. (2021). Double averaging analysis applied to a large eddy simulation of coupled turbulent overlying and porewater flow. *Water Resources Research*, *57*(11), e2021WR029918.

Lopez, F., & Garcia, M. (1997). *Open-channel flow through simulated vegetation: Turbulence modeling and sediment transport.* US Army Engineer Waterways Experiment Station.

Mackenthun, A. A., & Stefan, H. G. (1998). Effect of flow velocity on sediment oxygen demand: Experiments. *Journal of Environmental Engineering*, *124*(3), 222–230.

Manes, C., Pokrajac, D., McEwan, I., & Nikora, V. (2009). Turbulence structure of open channel flows over permeable and impermeable beds: A comparative

study. *Physics of Fluids*, *21*(12), 125109.
Manes, C., Ridolfi, L., & Katul, G. (2012). A phenomenological model to describe turbulent friction in permeable-wall flows. *Geophysical research letters*, *39*(14).
Marion, A., Bellinello, M., Guymer, I., & Packman, A. (2002). Effect of bed form geometry on the penetration of nonreactive solutes into a streambed. *Water Resources Research*, *38*(10), 27–1.
Miles, J. (2014). Tolerance and variance inflation factor. *Wiley statsref: statistics reference online*.
Motta, D., Abad, J. D., & García, M. H. (2010). Modeling framework for organic sediment resuspension and oxygen demand: case of bubbly creek in chicago. *Journal of Environmental Engineering*, *136*(9), 952–964.
Nagaoka, H., & Ohgaki, S. (1990). Mass transfer mechanism in a porous riverbed. *Water Research*, *24*(4), 417–425.
Nikora, V., McLean, S., Coleman, S., Pokrajac, D., McEwan, I., Campbell, L., ... Koll, K. (2007). Double-averaging concept for rough-bed open-channel and overland flows: Applications. *Journal of hydraulic Engineering*, *133*(8), 884–895.
O'Connor, B. L., & Harvey, J. W. (2008). Scaling hyporheic exchange and its influence on biogeochemical reactions in aquatic ecosystems. *Water Resources Research*, *44*(12).
O'Connor, B. L., & Hondzo, M. (2008). Dissolved oxygen transfer to sediments by sweep and eject motions in aquatic environments. *Limnology and Oceanography*, *53*(2), 566–578.
O'Connor, B. L., Hondzo, M., & Harvey, J. W. (2009). Incorporating both physical and kinetic limitations in quantifying dissolved oxygen flux to aquatic sediments. *Journal of Environmental Engineering*, *135*(12), 1304–1314.
OConnor, D. J. (1984). Turbulent transfer across smooth and rough surfaces. In *Gas transfer at water surfaces* (pp. 321–331). Springer.
Packman, A. I., Salehin, M., & Zaramella, M. (2004). Hyporheic exchange with gravel beds: Basic hydrodynamic interactions and bedform-induced advective flows. *Journal of Hydraulic Engineering*, *130*(7), 647–656.
Perry, A. E., Schofield, W. H., & Joubert, P. N. (1969). Rough wall turbulent boundary layers. *Journal of Fluid Mechanics*, *37*(2), 383–413.
Raupach, M., Antonia, R., & Rajagopalan, S. (1991). Rough-wall turbulent boundary layers.
Sakamoto, Y., Ishiguro, M., & Kitagawa, G. (1986). Akaike information criterion statistics. *Dordrecht, The Netherlands: D. Reidel*, *81*(10.5555), 26853.
Shaw, D. A., & Hanratty, T. J. (1977). Turbulent mass transfer rates to a wall for large schmidt numbers. *AIChE Journal*, *23*(1), 28–37.
Steinberger, N., & Hondzo, M. (1999). Diffusional mass transfer at sediment-water interface. *Journal of environmental engineering*, *125*(2), 192–200.
Stoesser, T., Frohlich, J., & Rodi, W. (2007). Turbulent open-channel flow over a permeable bed. In *Proceedings of the congress-international association for hydraulic research* (Vol. 32, p. 189).
Tonina, D., & Buffington, J. M. (2007). Hyporheic exchange in gravel bed rivers with pool-riffle morphology: Laboratory experiments and three-dimensional modeling. *Water Resources Research*, *43*(1).
Voermans, J. J., Ghisalberti, M., & Ivey, G. (2017). The variation of flow and turbulence across the sediment–water interface. *Journal of Fluid Mechanics*, *824*, 413–437.
Voermans, J. J., Ghisalberti, M., & Ivey, G. N. (2018a). The hydrodynamic response of the sediment-water interface to coherent turbulent motions. *Geophysical Research Letters*, *45*(19), 10–520.
Voermans, J. J., Ghisalberti, M., & Ivey, G. N. (2018b). A model for mass transport

across the sediment-water interface. *Water Resources Research*, *54*(4), 2799–2812.

Waterman, D., Liu, X., Motta, D., & García, M. H. (2016). Analytical lagrangian model of sediment oxygen demand and reaeration flux coevolution in streams. *Journal of Environmental Engineering*, *142*(7), 04016028.

Waterman, D., Waratuke, A., Motta, D., Cataño-Lopera, Y., & Garcia, M. H. (2009). Bubbly creek sediment oxygen demand (sod) study with the u of i hydrodynamic sod sampler. *Ven Te Chow Hydrosystems Laboratory, University of Illinois at Urbana–Champaign, Urbana, Ill*.

Waterman, D., Waratuke, A. R., Motta, D., Cataño-Lopera, Y. A., Zhang, H., & García, M. H. (2011). In situ characterization of resuspended-sediment oxygen demand in bubbly creek, chicago, illinois. *Journal of Environmental Engineering*, *137*(8), 717–730.

Wu, H., Zamalloa, C. C. Z., Landry, B. J., & Garcia, M. H. (2019). Experimental comparison of initiation of motion for submerged objects resting on fixed permeable and impermeable beds. *Physical Review Fluids*, *4*(1), 013802.

A unifying model for hyporheic oxygen mass transfer under a wide range of near-bed hydrodynamic conditions

Chieh-Ying Chen[1], Dimitrios K. Fytanidis[2], and Marcelo H. Garcia[3,4]

[1]Graduate Student, Ven Te Chow Hydrosystems Laboratory, Department of Civil and Environmental Engineering, University of Illinois at Urbana-Champaign, 205 North Mathews Ave., Urbana, IL 61801. Email: cyc2@illinois.edu

[2]Adjunct Research Assistant Professor, Ven Te Chow Hydrosystems Laboratory, Department of Civil and Environmental Engineering, University of Illinois at Urbana-Champaign, 205 North Mathews Ave., Urbana, IL 61801. Email: fytanid2@illinois.edu

[3]M.T. Geoffrey Yeh Endowed Chair and Director, Ven Te Chow Hydrosystems Laboratory, Department of Civil and Environmental Engineering, University of Illinois at Urbana-Champaign, 205 North Mathews Ave., Urbana, IL 61801. Email: mhgarcia@illinois.edu

[4]Centro Internacional de Estudios de Grandes Ros, Facultad de Ingeniera y Ciencias Hdricas, Universidad Nacional del Litoral, Santa Fe City, Santa Fe CP 3000, Argentina.

Key Points:

- We performed reanalysis of flume/field data combined with numerical results to develop models for the oxygen hyporheic mass exchange rate.
- We used a validated numerical model to expand the available dataset of hyporheic oxygen mass exchange under various bed and flow conditions.
- We proposed unifying single-parameter models for the estimation of hyporheic oxygen mass coefficient in open-channel flows.

Corresponding author: Chieh-Ying Chen, `cyc2@illinois.edu`

Abstract

Existing models for estimating hyporheic oxygen mass transfer often require numerous parameters related to flow, bed, and channel characteristics, which are frequently unavailable. We performed a meta-analysis on existing dataset, enhanced with high Reynolds number cases from a validated Computational Fluid Dynamics model, to identify key parameters influencing effective diffusivity at the sediment water interface. We applied multiple linear regression to generate empirical models for predicting eddy diffusivity. To simplify this, we developed two single-parameter models using either a roughness or permeability-based Reynolds number. These models were validated against existing models and literature data. The model using roughness Reynolds number is easy to use and can provide an estimate of the oxygen transfer coefficient, particularly in scenarios where detailed bed characteristics such as permeability might not be readily available.

Plain Language Summary

Current methods for estimating how oxygen is transferred in the sediment-water interface of rivers often require a lot of information about things like the flow and the riverbed characteristics. Unfortunately, this information is often not easy to get. We did a study looking at existing data from flume experiments and the field and added new data from a verified computational model. We wanted to identify which factors are most important in determining how much oxygen moves towards the bed at the sediment-water interface. Using some statistical mathematical tools, we came up with two simple models that only need one piece of information to make predictions. One model considers sediment size, the other looks at riverbed permeability. We validated these models by comparing them to existing methods and data from other studies, and they performed well. The model based on sediment size, which also reflects the roughness of the riverbed, performs best and is the most user-friendly because it does not require information about permeability, which is harder to estimate. This model can provide a reliable estimate of how oxygen moves at the sediment-water interface, particularly when specific details about the riverbed are not available.

1 Introduction

Dissolved oxygen (DO) is a critical component in aquatic ecosystems, impacting nutrient cycling, algae growth, aquatic life maintenance, and pollutant removal in water and sediment (Chapra, 2008). At the sediment-water interface (SWI), sediment oxygen demand (SOD) functions as an oxygen removal flux, transporting dissolved oxygen (DO) from the water to the sediment. This balances the penetration of DO caused by near-bed turbulence with the DO consumed by sediment and benthic chemical processes within the bed (Jørgensen & Revsbech, 1985; Gundersen & Jorgensen, 1990; Mackenthun & Stefan, 1998; Boudreau & Jorgensen, 2001). Accurate modeling of DO dynamics and oxygen mass transfer at the SWI is crucial for understanding nutrient cycling in riverine systems (Waterman et al., 2009; Motta et al., 2010; Waterman et al., 2011; Boano et al., 2014; Waterman et al., 2016).

In smooth-wall hyporheic flows, the oxygen mass transfer coefficient (K_L) is a function of DO diffusivity (D_{eff}) and diffusive layer thickness (δ_{DL}): $K_L = D_{eff}/\delta_{DL}$ at the SWI. K_L is affected by flow shear velocity (u_*), Reynolds number, bed roughness, and the momentum exchange due to hyporheic flow. O'Connor et al. (2009) summarized data for K_L from the literature collected over hydrodynamically smooth beds (Shaw & Hanratty, 1977; Dade, 1993; Steinberger & Hondzo, 1999; Hondzo et al., 2005; Arega & Lee, 2005; O'Connor & Hondzo, 2008) and expressed the dimensionless mass transfer coefficient (K_{L+}) as a function of a temperature-dependent Schmidt number (S_c): $K_{L+} = K_L/u_* = \alpha S_c^{\beta}$, with ranges for α and β being 0.052 to 0.164 and -0.704 to -0.67, respectively. K_{L+} has Reynolds number dependence at low and moderate Reynolds number flows and reaches a self-similar plateau value for large enough Reynolds numbers (Shaw & Hanratty, 1977; Steinberger & Hondzo, 1999).

High roughness height, bed permeability (Perry et al., 1969; Raupach et al., 1991; Jiménez, 2004; Wu et al., 2019), and bed forms (Elliott & Brooks, 1997; Marion et al., 2002; Packman et al., 2004; Tonina & Buffington, 2007) can also enhance hyporheic momentum exchange and thus the mass transfer by increasing the shear stress at the SWI. Han et al. (2018) summarized K_{L+} values from experimental studies over rough beds and found that rough bed K_{L+} values can be up to two orders of magnitude higher than those over smooth beds (Nagaoka & Ohgaki, 1990; Inoue & Nakamura, 2011; Han et al., 2018). OConnor (1984) studied the transfer coefficient for open-channel flows with smooth and rough beds and proposed an analytical equation for the transitional regime. δ_{DL} values are difficult to be estimated for the case of rough wall. Thus, different length scales may be used as flow characteristic length scales at the SWI of rough walls. Nagaoka and Ohgaki (1990) adopted a pore scale restricted mixing length $B = \frac{2\phi^2}{3(1-\phi)}D$ for the estimation of D_{eff} at the SWI. Manes et al. (2012) and Voermans et al. (2017) proposed flow length scales associated with characteristic turbulent eddy size across the SWI (δ_p^*) and the depth of turbulent shear penetration in the bed (δ_p) respectively. Another relevant length scale is the vertical location of the inflection point in the mean velocity profile δ (where $\frac{dU^2}{dz^2} = 0$ and $\frac{d<\overline{U}>}{dz}$ is maximum) which also corresponds to the position of the SWI defined with respect to the top of the sediments (Voermans et al., 2017).

Experimental studies using Particle Image Velocimetry (PIV) (Goharzadeh et al., 2005; Manes et al., 2009; Voermans et al., 2017; Kim et al., 2018; Wu et al., 2019; Kim et al., 2020) have examined the effect of Reynolds number, bed roughness, and bed permeability on eddy viscosity and diffusivity at the SWI. The flow structure at the SWI and inside the bed has been studied numerically using Direct Numerical Simulation (DNS) (Breugem & Boersma, 2005; Breugem et al., 2006; Kuwata & Suga, 2019) and Large Eddy Simulation (LES) (Stoesser et al., 2007; Han et al., 2018; He et al., 2019; Lian et al., 2019, 2021) models. Different scaling parameters for modeling the effective oxygen diffusivity have been proposed by these studies, including bulk Reynolds number (Packman et al., 2004), roughness Reynolds number, and permeability-based Reynolds and Peclet numbers (Grant et al., 2012; Voermans et al., 2017, 2018b). O'Connor and Harvey (2008) summarized the different modes of hyporheic exchange (molecular diffusion, bioturbation, advection, shear, bed mobility, and turbulence) and developed a scaling relationship for the effective diffusion coefficient (D_{eff}) based on a roughness Reynolds number ($Re_* = k_s u_*/\nu$, where u_* is the shear velocity and k_s is roughness height) with a permeability-based Peclet number ($Pe_k = \sqrt{K}u_*/D_m$, K is bed permeability and D_m is the molecular diffusivity). Grant et al. (2012) used both inner and outer scales combined with multiple linear regression (MLR) over an extensive dataset from the literature and found that D_{eff}/D_m has a strong relationship with permeability Reynolds number ($Re_k = \sqrt{K}u_*/\nu$), a Reynolds number defined using the bed thickness ($Re_{H_b} = H_b u_*/\nu$), and porosity ϕ. Voermans et al. (2017, 2018b) conducted a series of experiments across different ranges of permeability, showing the dependencies of D_{eff}/D_m, δ_p and δ_{p*} on Re_k. They also identified a critical Re_k value (Re_k ~1-2) above which turbulence exchange effects dominate over dispersion at the SWI. Finally, the Re_k and Re_* values for these analyses range between $0.01 - 10$ and $1 - 10^4$, respectively.

However, in practice, an ***a priori*** estimation or measurement of permeability can be challenging. Additional experimental tests, e.g., Darcy's permeability measurement (Darcy, 1856), or correlations and analytical expressions between different bed parameters, e.g., the KozenyCarman model (Kozeny, 1927; Bear, 1972), are required for permeability estimation.

In our work, we focused on extending the analysis previously done for the scaling and modeling of effective diffusivity, estimating oxygen mass transfer coefficient, and developing new simple relationships for the estimation of these parameters in practice. We used a computationally efficient method, IDDES (Improved Delayed Detached Eddy Simulations), to extend the range of previously reported Re_k and Re_* in ranges that measurements are not available to date. The numerical results were compared and validated against data from the literature. We also performed a reanalysis and MLR using data from the literature combined with our numerical results to reexamine the relationships between D_{eff}/D_m and inner and outer-/bulk parameters of the bed and the flow. Finally, novel unifying single-parameter models for the prediction of oxygen mass transfer coefficient using roughness or permeability scales were proposed, based on Re_k and Re_*. The proposed models can accurately predict data from field and laboratory conditions from the literature.

2 Definitions

The vertical hyporheic oxygen exchange flux ($J_{S_{O_2}}$) at the SWI is shown in Figure 1 along with the definitions of the primary parameters influencing it. These parameters include the bulk and near-bed hydrodynamics (U_b, u_*, k_s, H_w) as well as the SWI and porous sediment bed characteristics (K, ϕ, H_b). The total/effective mass flux comprises molecular ($J^{MD}_{S_{O_2}}$), dispersive ($J^{DIS}_{S_{O_2}}$), and turbulent ($J^{T}_{S_{O_2}}$) fluxes, which can be expressed as (Voermans et al., 2018b):

$$J_{S_{O_2}} = J^{MD}_{S_{O_2}} + J^{DIS}_{S_{O_2}} + J^{T}_{S_{O_2}} = -D_m \frac{d\phi < C >}{dz} + \phi < \tilde{w}\tilde{C} > + \phi < \overline{w'C'} > \qquad (1)$$

The quantities mentioned above utilize Reynolds and spatial decompositions: $\psi = \overline{\psi} + \psi'$ and $\overline{\psi} = < \overline{\psi} > + \tilde{\psi}$, in which the variable ψ is represented by overbarred, primed, bracketed, and tilded quantities. These indicate the time-averaged, time-fluctuating, spatially-averaged, and spatial-fluctuating quantities, respectively (Lopez & Garcia, 1997; Nikora et al., 2007; Voermans et al., 2018b).

In this study, we performed IDDES simulations on theoretical cases, employing surrogate beds composed of closely packed, monodisperse spheres, as in previous research examining hyporheic mass exchange (Stoesser et al., 2007; Manes et al., 2009; Wu et al., 2019) (Figures 1a and b). Figure 1b illustrates typical normalized streamwise velocity (u_x) by shear velocity (u_*), while the average velocity profile is depicted in Figure 1c. The inflection point (δ) (Figure 1d) in the streamwise velocity profile signifies the extrusion of bed-penetrating eddies and the virtual "interface" of the bed (Manes et al., 2012; Voermans et al., 2018b). Figure 1c shows typical shear stresses as they are computed by the deployed numerical method: $\tau_{total} = \tau_\nu + \tau_{RS} + \tau_{form}$ (Nikora et al., 2007), where τ_{total} is estimated as the integral of viscous and drag forces over the top hemispheres and follows a linear profile until $\tau_{total} = 0$ at $z = H_w$ as $\tau_{total} = \tau_{bed}(1 - z/H_w)$ ($\tau_{bed} = \tau_{total}(z_{bed}) = \int_A F_{viscous} + F_{pressure} dA$, where A is the area of the bed above z=0), $\tau_\nu = \mu d < \overline{u} > /dz$ is the viscous stresses, τ_{RS} is the sum of resolved and modeled Reynolds stresses, and τ_{form} is the form-induced stresses.

This length scale (δ) is preferred over penetration length scale (δ_p) and total height (δ_{p*}) due to its independence from the need for endoscopic measurement techniques (Blois et al., 2014) or refractive index matching (Voermans et al., 2017), even though porous bed permeability still influences δ. Later in the paper, we capitalize on the benefits of δ to create an easy-to-use predictor for hyporheic mass exchange under a variety of flow and bed conditions.

3 Computational Fluid Dynamics Solver

Using the Detached Eddy Simulation (DES) approach, we expanded our dataset via 3D hydrodynamic simulations of hyporheic boundary layer flows with OpenFOAM. We employed the PIMPLE algorithm for incompressible 3D Navier-Stokes equations and

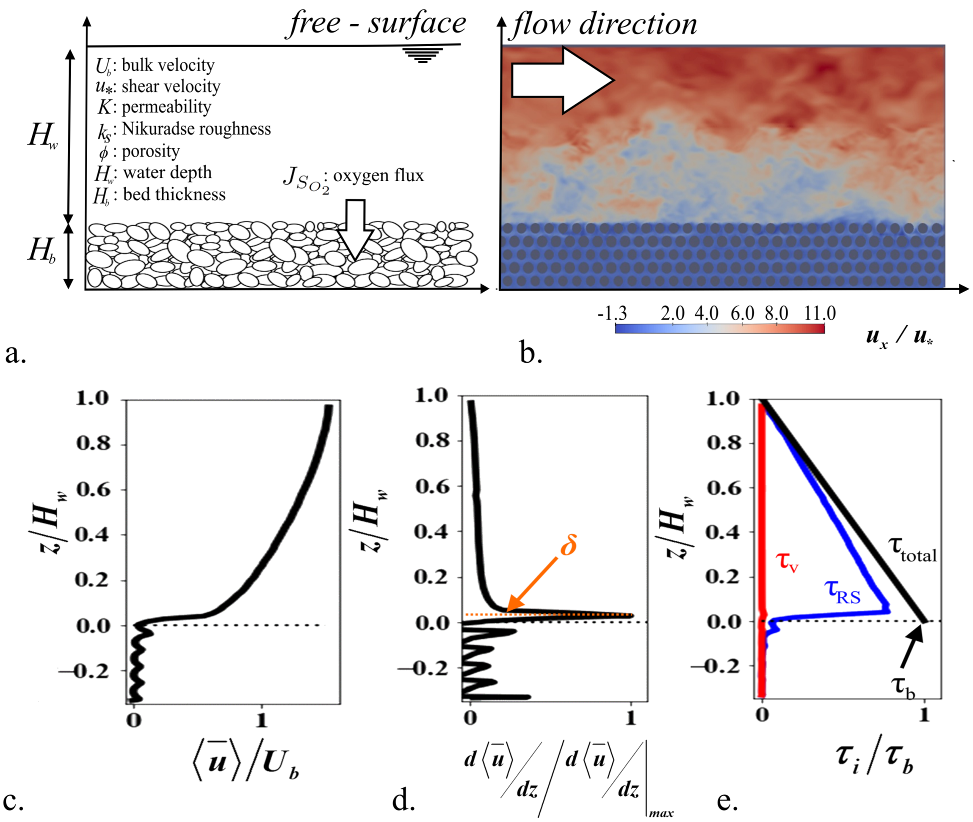

Figure 1. (a) Schematic plot of the problem and definition of quantities, (b) instantaneous u_x/u_* over the surrogate bed, (c) ensembled average velocity profile, (d) normalized ensembled velocity gradient, (e) shear stress distribution.

applied the Spalart-Allmaras Improved Delayed Detached Eddy Simulation (SA-IDDES) for modeling ν_{eff}. The equations of motion were solved assuming that the flows were both incompressible and isothermal. This model was validated using benchmark hyporheic flow cases, compared against Smagorinsky LES model simulations and literature data. We performed detailed analysis to establish result independence considering domain size, boundary conditions, mesh resolutions, and integration time (see supporting information for details - SI1). Figures 2a-d summarize the comparisons of one of the simulations performed herein in dashed lines for the mean velocity (U_x), Reynolds stresses ($\sqrt{\overline{u'w'}}/u_*$) and the variances ($\sigma_u/u_*$ and σ_w/u_*) with measurements performed by Manes et al. (2009) for five-layer low-Re case (Re_k=31.2) and the LES results by Lian et al. (2021) for Re_k=24.2. Table 1 in supporting information - SI2 summarizes all the cases that have been examined in the present study, aiming to expand the existing dataset for high Reynolds number and roughness cases. Also, in Figures 2c and d the similarity relations introduced by Ghisalberti (2009) for a wide range of obstructed shear flows are shown using dashed gray lines. Figures 2e and f show the normalized $\delta u_*/\nu$ thickness as it compares with the corresponding data in Voermans et al. (2018b) as functions of Re_k and Re_*, where $Re_* = k_s u_*/\nu$ with k_s=2.5D (Note that $\delta = \delta_{p*} - \delta_p$). δ is approximately $\sim$0.145$\times$2.5D=0.36D which is reasonably close to the 0.3 value reported by Voermans et al. (2017). Figures 2g and h show the mixing-length ($< L_m >= \sqrt{< \overline{u'w'} > /(dU/dz)^2}$) as functions of Re_k and Re_*. The predictions are reasonably close to those by Voermans et al. (2018b).

4 Hyporheic Mass Exchange Rate and Effective Diffusivity

The effective diffusivity (D_{eff}) can be used to parameterize mass hyporheic exchange under the assumption that the mass transport of oxygen in the sediment bed can be modeled by Ficks second law, which can be expressed for homogeneous porous mediums as (Grant et al., 2012):

$$\frac{d\phi C_{O_2}}{dt} = \frac{d}{dz}\left(\phi D_{eff}\frac{dC_{O_2}}{dz}\right) \tag{2}$$

The oxygen flux at the SWI which is a boundary conditions for the above equation is defined as (O'Connor & Harvey, 2008; O'Connor et al., 2009):

$$J_{S_{O_2}} = -D_{eff}\frac{dC_{O_2}}{dz}|_{z=0} = -(D_m + D_{dis} + D_t)\frac{dC_{O_2}}{dz}|_{z=0} = \frac{D_{eff}}{\delta_{DL}}(C_{w_{O_2}} - C_{s_{O_2}}) \tag{3}$$

In Figure 1a, we defined the oxygen flux ($J_{S_{O_2}}$) which under equilibrium should balance the oxygen consumed within the sediment bed by chemical processes. This mass exchange flux includes the effect of molecular (D_m), dispersive (D_{dis}) and turbulent (D_t) diffusivities (Voermans et al., 2018b). For the case of smooth beds, D_{eff}/δ_{DL} are typically used for the computation of the oxygen flux. In our model we will replace δ_{DL} with inflection point δ, which can be estimated using our numerical results and from empirical equations $\delta_{p*}u_*/\nu = 22Re_k^{1.2}$ and $\delta_p u_*/\nu = 8Re_k^{1.8}$ introduced by Voermans et al. (2018b).

5 Analysis and Results

5.1 Parameterization for D_{eff}

We followed a similar approach as O'Connor and Harvey (2008) and Grant et al. (2012) for parameterizing the effective diffusivity (D_{eff}). Specifically, we used Buckingham's Pi theorem to create dimensionless groupings of the controlling independent variables, as demonstrated in O'Connor and Harvey (2008) and Grant et al. (2012):

$$D_{eff} = f(\nu, D_m, H_w, H_b, U_b, u_*, k_s, K, \phi) \tag{4}$$

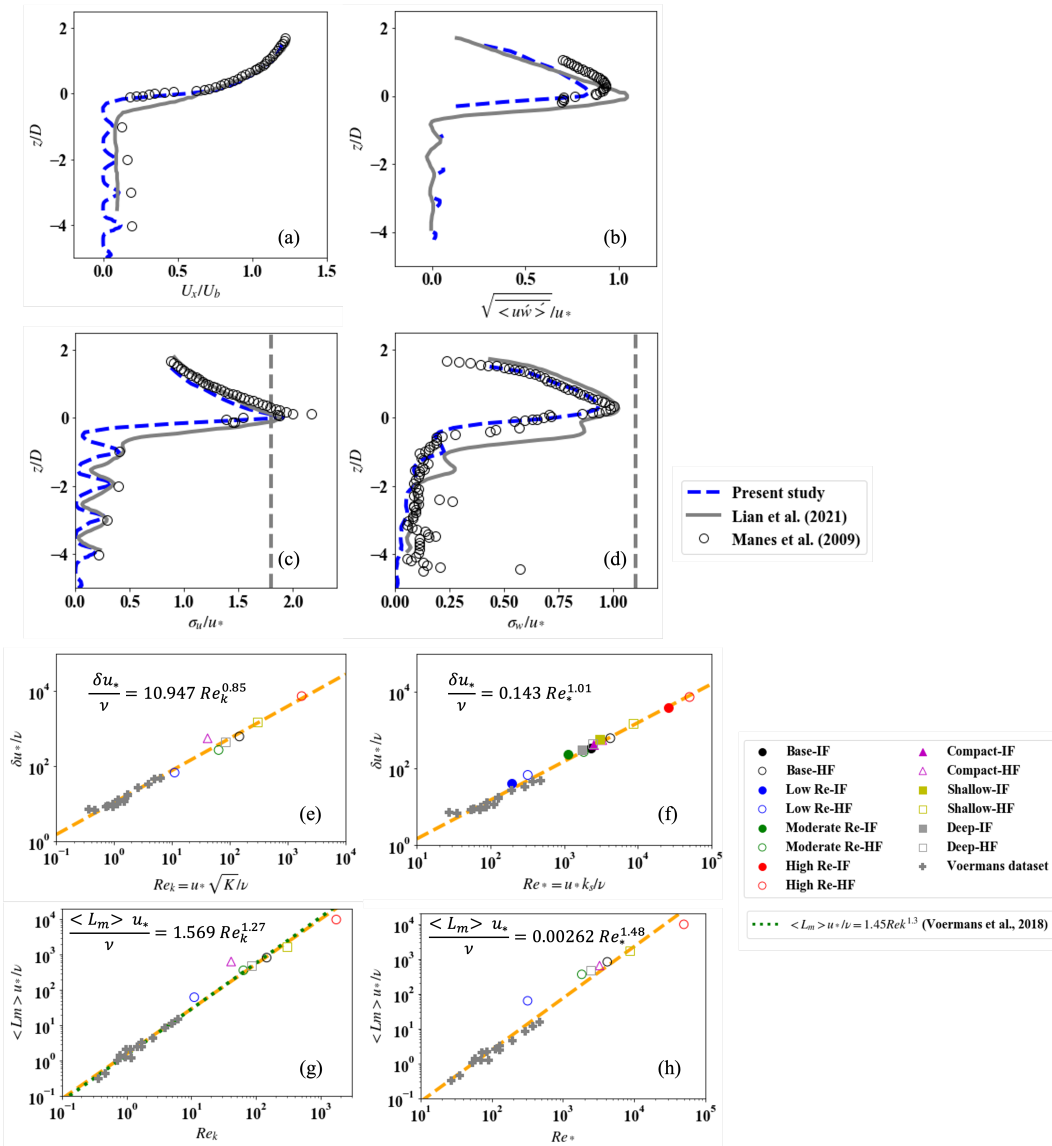

Figure 2. (a), (b), (c) and (d) Typical CFD results and comparison against data from the literature for U_x/U_b, $\sqrt{<\overline{u'w'}>}/u_*$, σ_u/u_* and σ_w/u_*. (e), (f), (g) and (h) fitting relations of length scale δ and mixing length $<L_m>$ with Re_k and Re_*.

In the equation above, there are nine variables (n=9) and two primary dimensions (L, T), m=2. Consequently, a predictive equation for effective diffusivity should have a maximum of seven (n-m=7) non-dimensional groups. For our analysis, we propose that a normalized D_{eff}/D_m can be predicted as a function of the following dimensionless parameters:

$$\frac{D_{eff}}{D_m} = f(Re_{bulk} = \frac{U_b H_w}{\nu}, Re_{Hw} = \frac{u_* H_w}{\nu}, Re_{H_b} = \frac{u_* H_b}{\nu}, Re_* = \frac{u_* k_s}{\nu}, \\ Re_k = \frac{u_* \sqrt{K}}{\nu}, Pe_k = \frac{u_* \sqrt{K}}{D_m}, \phi) \tag{5}$$

Eq.(5) has the potential to account for bulk and near sediment bed hydrodynamic effects (Re_{bulk}, Re_*), SWI exchange (Re_k, Pe_k, ϕ), and flume facility/computational-domain size dependencies (Re_{H_w},Re_{Hb}).

Assuming a power law model (Grant et al., 2012) for modeling the dependence of the equation on the above parameters, we can write:

$$log\frac{D_{eff}}{D_m} = \alpha + \beta log Re_{bulk} + \gamma log Re_{Hw} + \delta log Re_{H_b} + \epsilon log Re_* + \varepsilon log Re_k + \zeta log Pe_k + \eta log\phi \tag{6}$$

We used a multiple linear regression (MLR) methodology, following approach used by Grant et al. (2012), to develop a model based on the available data from the literature. This dataset integrates field and flume data from earlier studies (O'Connor & Harvey, 2008; Grant et al., 2012; Voermans et al., 2018b) along with our numerical results. The dataset details are supplied in the supporting information - SI3 and this is the foundation for model development. In testing the possible models, we experimented with 255 different combinations of seven parameters, along with a constant α. The procedure of MLR necessitates that the dependent variable be defined as functions of a group of independent variables, which must not be highly correlated. Thus, it was crucial to initially examine the linearity between dependent and independent variables and then to verify the correlation between chosen independent variables.

Following the approach by Grant et al. (2012), we used the variance inflation factor (VIF) to rule out combinations with high-correlated parameters (Miles, 2014). The VIF is an index indicating the extent to which a given variable is influenced by the variation in other variables. A VIF of 1 signifies no correlation, whereas a higher VIF suggests increased correlation. To strike a balance between model complexity and accuracy, Grant et al. (2012) recommended the use of a combination that excludes any variables with VIF>5 and employs the Akaike information criterion (AIC) as the selection criterion. The AIC estimates the degree of information loss in a model (Akaike, 1974; Sakamoto et al., 1986; Aho et al., 2014). We applied the VIF as a filtering mechanism and the minimum AIC as a selection standard. Table 4 in the supporting information - SI4 summarizes the 5 models with the best fitness to the training data.

Figures 3a, b and c show the fitness of the 3 best performing models. In an effort to develop a simple single-parameter model for all different bed and flow characteristics, D_{eff}/D_m versus every single of the 6 dimensionless numbers considered in our MLR analysis are plotted in Figures 3d-i together with the corresponding R^2 values. It is shown that Re_k and Re_* show the best coefficient of determination, which will be explored as single parameters to develop empirical model for the prediction of the oxygen mass transfer coefficient.

5.2 A unifying model for the hyporheic oxygen mass transfer

In the previous paragraph, we established the best single-parameter models for D_{eff}/D_m based on roughness Reynolds number (Re_*) and permeability Reynolds number (Re_k),

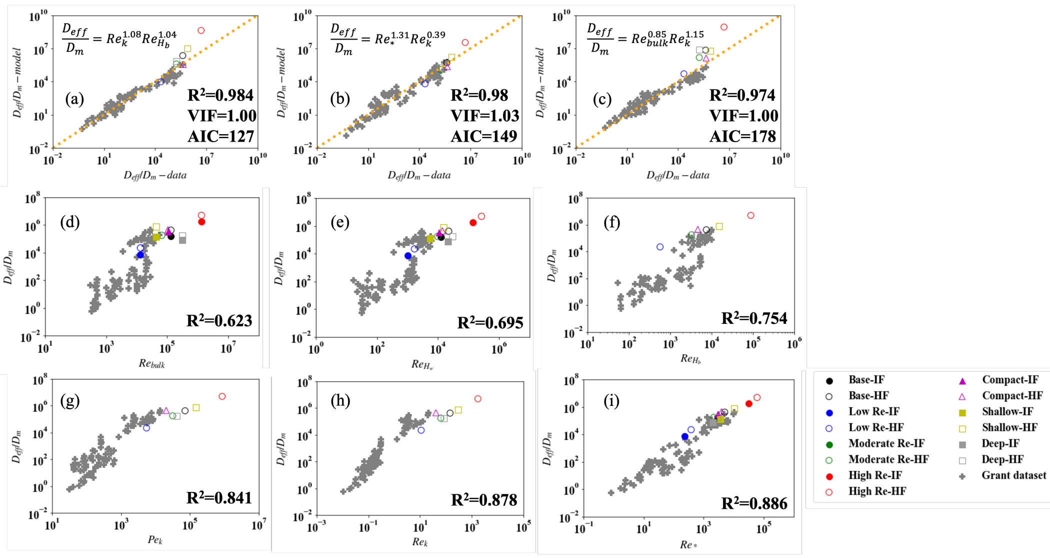

Figure 3. (a), (b), (c) D_{eff}/D_m evaluation of the three best performing MLR models: $Re_k^{1.08}Re_{H_b}^{1.04}$, $Re_*^{1.31}Re_k^{0.39}$, $Re_{bulk}^{0.85}Re_k^{1.15}$. (d), (e), (f), (g), (h), (i) prediction ability by single parameter models: Re_{bulk}, Re_{Hw}, Re_{Hb}, Pe_k, Re_k, Re_*.

given their highest R^2 values. Using these Reynolds numbers, we were able to scale the mass transfer coefficient K_L, forming a new relationship for oxygen mass transfer across diverse roughness and permeability conditions. To address the problem of defining the diffusive layer (δ_{DL}) in rough wall situations, we introduced a unifying transfer coefficient, $\tilde{K_L} = D_{eff}/\delta$ and $\tilde{K_L^+} = \tilde{K_L}/u_*$, applicable to both hydrodynamically smooth and rough cases. This is done using the inflection point δ which can be estimated for all conditions using the equations in Figure 2.

The functions we proposed, represented as $\tilde{K_L^+} = \alpha Re_i^\beta/(Re_i^\beta + \gamma)$, where $Re_i = Re_*$ or Re_k, take inspiration from the sediment entertainment function by Garcia and Parker (1991). These functions describe how $\tilde{K_L^+}$ starts from zero and increases with Re_* and Re_k until it plateaus at higher Re_* and Re_k, aligning with self-similar plateau values proposed by Shaw and Hanratty (1977) and Steinberger and Hondzo (1999).

We used data from O'Connor et al. (2009), Han et al. (2018) and Voermans et al. (2018b), dataset that include smooth to fully rough beds and low to high permeabilities (Steinberger & Hondzo, 1999; O'Connor & Hondzo, 2008; O'Connor et al., 2009; Nagaoka & Ohgaki, 1990; Elliott & Brooks, 1997; Marion et al., 2002; Packman et al., 2004; Tonina & Buffington, 2007; Voermans et al., 2017). All data can be found in Table 5 in the supporting information - SI5. Following regression analysis, we derived two equations, with results displayed in Figures 4a and b:

$$\tilde{K_L^+} = \frac{2.058 Re_*^{0.698}}{Re_*^{0.698} + 412.949} = \frac{2.045 Re_k^{0.729}}{Re_k^{0.729} + 31.973} \tag{7}$$

To validate the accuracy of our model, we tested it against the data used for the MLR. We also used the zonal model by Voermans et al. (2018b) to predict using the same dataset. Note that this dataset is the same one used by Voermans et al. (2018b) for their

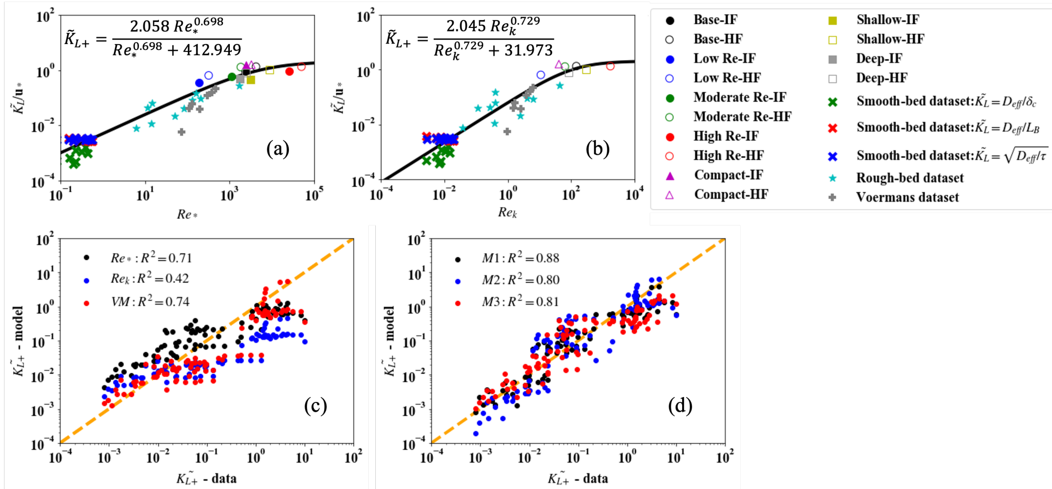

Figure 4. (a), (b) Non-dimensional $\tilde{K_L^+}$ versus Re_* and Re_k. (c) Evaluation of the accuracy of the two proposed models and comparison against zonal model in Voermans et al. (2018b). (d) Evaluation of the three best performing models based on the MLR analysis.

regression. Voermans et al. (2018b)'s zonal model is represented as:

$$\frac{D_{eff}}{D_m} = \begin{cases} 1 & Re_k \leq 0.02 \\ 1.6 Re_k^2 S_c & 0.02 < Re_k < 1 \\ 1.9 Re_k^2 S_c & Re_k \geq 1 \end{cases} \tag{8}$$

The δ values were estimated from closure equations depicted in Figure 2, and the D_m, u_*, k_s, and K values are available for all cases. The performance of the two unified equations proposed in this study is shown in Figure 4c.

The roughness-based Reynolds number model demonstrates a higher R^2 value (0.71) than the permeability-based Reynolds number model (0.42). Voermans et al. (2018b)'s zonal model shows an R^2 value of 0.74, quite close to the Re_*-based model, despite being derived from the validation dataset. Lastly, the three best performing models derived using MLR are also tested against the same dataset (see Figure 4d). As expected, the multi-parameter models proposed here outperform both the single-parameter models and the zonal model by Voermans et al. (2018b), with R^2 values of 0.88, 0.80, and 0.81 respectively.

A big advantage of the unifying model based on Re_* is the fact that it is solely based on the Nikuradse roughness height rather than permeability, which can potentially be more challenging parameter to estimate, i.e. the use of laboratory tests. In fact, even if compared with the prediction by Voermans et al. (2018b)'s zonal model (mean absolute error is 1.05), the MAE is 1.19 for the Re_*-based model while the MAE for the Re_k-based model is 1.66. Finally, the 3 MLR models have typically smaller errors (0.73, 0.97, 0.94 respectively); however, they introduce additional complexity and in some cases, i.e. $D_{eff}/D_m = Re_k^{1.076} Re_{H_b}^{1.038}$, parameters like the thickness of the bed permeable layer (H_b) in Re_{H_b} have more importance when we study the oxygen exchange at a laboratory setting using shallow test flumes or require significant field work to estimate the elevation of any impervious bedrock layer.

6 Applications and Relevant Discussions of the Single-parameter Model

The proposed Re_*-based model outlined earlier requires minimal data inputs. These include some parameter estimations:

- Nikuradse roughness (k_s) can be determined based on characteristic bed diameters as $k_s = \alpha_s D_s$, where D_s could be D_{50} or D_{70}. A comprehensive list of α_s values can be referred to Garcia (2008). For example, $k_s = \alpha_s D_s$=2.5D_{50}.
- Shear velocity (u_*) can be estimated by the friction slope (S_f) data as $u_* = \sqrt{gH_w S_f}$, or referred to nomographs and models for hyporheic friction factors, such as those in Manes et al. (2012) and Voermans et al. (2018a).
- Length scale δ can be calculated by the equations in Figure 2 as $\delta u_*/\nu = 0.143 Re_*^{1.01}$ ($\delta \sim$0.143k_s).
- Kinematic viscosity (ν) is a temperature relevant parameter. The ν of water can be estimated using the formula: $\nu = 1.79 \times 10^{-6}/(1 + 0.3368T_c + 0.00021T_c^2)$ with T_c in Celsius.

With the parameters above, $\tilde{K_L}$ can be obtained from Equation (7) by $Re_* = k_s u_*/\nu$ and u_*. The effective oxygen diffusivity can be determined as $D_{eff} = \tilde{K_L}\delta$.

If you have permeability measurements, you can utilize either the Re_k-based model by Re_k in Equation (7) or the zonal model by (Voermans et al., 2018b). The MLR-based models shown in Figure 3 can also estimate D_{eff}/D_m when both k_s and K data are available. If additional data such as the thickness of a permeable layer (H_b) atop an impermeable bottom or other bed thickness restrictions (for instance, in laboratory flume flow cases) are available, you can also use the MLR-derived model based on $Re_{Hb} = u_* H_b/\nu$.

It's crucial to note that the unifying model from Equation (7) can yield D_{eff} values that are smaller than the molecular diffusivity (D_m). This typically occurs in low Reynolds number flows where oxygen mass exchange is primarily driven by molecular diffusion, a less common scenario in open-channel cases. Instances with ratios as low as D_{eff}/D_m=0.6 were reported by Grant et al. (2012) and Voermans et al. (2018b) may have documented cases resulting from tortuosity effects between grains (O'Connor & Harvey, 2008). Voermans et al. (2018b) noted that D_{eff} equals D_m for Re_k less than 0.02 (see Equation (8)). O'Connor and Harvey (2008) suggested a similar criterion of $Re_* Pe_k^{6/5}$ <2000 which leads to $D_{eff} = D_m$ for a tortuosity parameter β=1. The models developed here can be adjusted to consider these criteria by introducing a limiting parameter where D_{eff} is the maximum of the predicted value and D_m (or βD_m if considering tortuosity effects).

7 Conclusion

A meta-analysis of pre-existing datasets, supplemented by high Reynolds number Computational Fluid Dynamics (CFD) results, was conducted to examine the scaling parameters that influence oxygen mass transfer in hyporheic zones. Using this enhanced dataset, multiple linear regression was utilized to create multi-parameter predictive models for effective diffusivity in turbulent hyporheic flows. A novel unifying model was then introduced, aiming to estimate the oxygen mass transfer coefficient using the roughness height rather than bed permeability. This newly developed model underwent validation through comparisons with other models and existing literature data. It is designed to serve as a user-friendly tool that can provide essential data for estimating the oxygen transfer coefficient, particularly in scenarios where detailed bed characteristics might not be readily available.

Data Availability Statement

All numerical results in this manuscript were generated by Openfoam v8 (`https://openfoam.org/version/8/`). Data archiving is underway. The Openfoam setup and numerical results are temporarily uploaded as Supporting Information for review purposes. All the data will be uploaded to Zenodo data repository.

Acknowledgments

The financial support by Metropolitan Water Reclamation District of Greater Chicago (MWRDGC) is gratefully acknowledged. The computational support by National Science Foundation via grant number ACI-1548562 for Extreme Science and Engineering Discovery Environment (XSEDE), now migrated to Advanced Cyberinfrastructure Coordination Ecosystem: Services and Support (ACCESS), is appreciated. This work used XSEDE Stampede2 at the Texas Advanced Computing Center (TACC) through allocation TG-CTS190067 and Frontera at TACC through Pathways allocation CTS22005.

References

Aho, K., Derryberry, D., & Peterson, T. (2014). Model selection for ecologists: the worldviews of aic and bic. *Ecology*, *95*(3), 631–636.

Akaike, H. (1974). A new look at the statistical model identification. *IEEE transactions on automatic control*, *19*(6), 716–723.

Arega, F., & Lee, J. H. (2005). Diffusional mass transfer at sediment–water interface of cylindrical sediment oxygen demand chamber. *Journal of Environmental Engineering*, *131*(5), 755–766.

Bear, J. (1972). *Dynamics of fluids in porous media.* Elsevier, New York.

Blois, G., Best, J. L., Sambrook Smith, G. H., & Hardy, R. J. (2014). Effect of bed permeability and hyporheic flow on turbulent flow over bed forms. *Geophysical Research Letters*, *41*(18), 6435–6442.

Boano, F., Harvey, J. W., Marion, A., Packman, A. I., Revelli, R., Ridolfi, L., & Wörman, A. (2014). Hyporheic flow and transport processes: Mechanisms, models, and biogeochemical implications. *Reviews of Geophysics*, *52*(4), 603–679.

Boudreau, B. P., & Jorgensen, B. B. (2001). *The benthic boundary layer: Transport processes and biogeochemistry.* Oxford University Press.

Breugem, W.-P., Boersma, B., & Uittenbogaard, R. (2006). The influence of wall permeability on turbulent channel flow. *Journal of Fluid Mechanics*, *562*, 35.

Breugem, W.-P., & Boersma, B.-J. (2005). Direct numerical simulations of turbulent flow over a permeable wall using a direct and a continuum approach. *Physics of fluids*, *17*(2), 025103.

Chapra, S. C. (2008). *Surface water-quality modeling.* Waveland press.

Dade, W. B. (1993). Near-bed turbulence and hydrodynamic control of diffusional mass transfer at the sea floor. *Limnology and Oceanography*, *38*(1), 52–69.

Darcy, H. (1856). *Les fontaines publiques de la ville de dijon: exposition et application des principes à suivre et des formules à employer dans les questions de distribution d'eau... un appendice relatif aux fournitures d'eau de plusieurs villes au filtrage des eaux* (Vol. 1). Victor Dalmont, éditeur.

Elliott, A. H., & Brooks, N. H. (1997). Transfer of nonsorbing solutes to a streambed with bed forms: Laboratory experiments. *Water Resources Research*, *33*(1), 137–151.

Engelund, F. (1970). Instability of erodible beds. *Journal of Fluid Mechanics*, *42*(2), 225–244.

Garcia, M. (2008). *Sedimentation engineering: processes, measurements, modeling, and practice. asce manuals and reports on engineering practice no. 110. a.* American Society of Civil Engineers. Reston, VA.

Garcia, M., & Parker, G. (1991). Entrainment of bed sediment into suspension. *Journal of Hydraulic Engineering*, *117*(4), 414–435.
Ghisalberti, M. (2009). Obstructed shear flows: similarities across systems and scales. *Journal of Fluid Mechanics*, *641*, 51–61.
Goharzadeh, A., Khalili, A., & Jørgensen, B. B. (2005). Transition layer thickness at a fluid-porous interface. *Physics of Fluids*, *17*(5), 057102.
Grant, S. B., Stewardson, M. J., & Marusic, I. (2012). Effective diffusivity and mass flux across the sediment-water interface in streams. *Water Resources Research*, *48*(5).
Gundersen, J. K., & Jorgensen, B. B. (1990). Microstructure of diffusive boundary layers and the oxygen uptake of the sea floor. *Nature*, *345*(6276), 604–607.
Han, X., Fang, H., He, G., & Reible, D. (2018). Effects of roughness and permeability on solute transfer at the sediment water interface. *Water research*, *129*, 39–50.
He, G., Han, X., Fang, H., Reible, D., & Huang, L. (2019). Effects of roughness reynolds number on scalar transfer mechanisms at the sediment-water interface. *Water Resources Research*, *55*(8), 6811–6824.
Hondzo, M., Feyaerts, T., Donovan, R., & O'Connor, B. L. (2005). Universal scaling of dissolved oxygen distribution at the sediment-water interface: A power law. *Limnology and oceanography*, *50*(5), 1667–1676.
Inoue, T., & Nakamura, Y. (2011). Effects of hydrodynamic conditions on do transfer at a rough sediment surface. *Journal of Environmental Engineering*, *137*(1), 28–37.
Jiménez, J. (2004). Turbulent flows over rough walls. *Annu. Rev. Fluid Mech.*, *36*, 173–196.
Jørgensen, B. B., & Revsbech, N. P. (1985). Diffusive boundary layers and the oxygen uptake of sediments and detritus. *Limnology and oceanography*, *30*(1), 111–122.
Kim, T., Blois, G., Best, J. L., & Christensen, K. T. (2018). Experimental study of turbulent flow over and within cubically packed walls of spheres: Effects of topography, permeability and wall thickness. *International Journal of Heat and Fluid Flow*, *73*, 16–29.
Kim, T., Blois, G., Best, J. L., & Christensen, K. T. (2020). Experimental evidence of amplitude modulation in permeable-wall turbulence. *Journal of Fluid Mechanics*, *887*.
Kozeny, J. (1927). Uber kapillare leitung der wasser in boden. *Royal Academy of Science, Vienna, Proc. Class I*, *136*, 271–306.
Kuwata, Y., & Suga, K. (2019). Extensive investigation of the influence of wall permeability on turbulence. *International Journal of Heat and Fluid Flow*, *80*, 108465.
Lian, Y. P., Dallmann, J., Sonin, B., Roche, K., Liu, W. K., Packman, A., & Wagner, G. J. (2019). Large eddy simulation of turbulent flow over and through a rough permeable bed. *Computers & Fluids*, *180*, 128–138.
Lian, Y. P., Dallmann, J., Sonin, B., Roche, K. R., Packman, A. I., Liu, W. K., & Wagner, G. J. (2021). Double averaging analysis applied to a large eddy simulation of coupled turbulent overlying and porewater flow. *Water Resources Research*, *57*(11), e2021WR029918.
Lopez, F., & Garcia, M. (1997). *Open-channel flow through simulated vegetation: Turbulence modeling and sediment transport.* US Army Engineer Waterways Experiment Station.
Mackenthun, A. A., & Stefan, H. G. (1998). Effect of flow velocity on sediment oxygen demand: Experiments. *Journal of Environmental Engineering*, *124*(3), 222–230.
Manes, C., Pokrajac, D., McEwan, I., & Nikora, V. (2009). Turbulence structure of open channel flows over permeable and impermeable beds: A comparative

study. *Physics of Fluids*, *21*(12), 125109.
Manes, C., Ridolfi, L., & Katul, G. (2012). A phenomenological model to describe turbulent friction in permeable-wall flows. *Geophysical research letters*, *39*(14).
Marion, A., Bellinello, M., Guymer, I., & Packman, A. (2002). Effect of bed form geometry on the penetration of nonreactive solutes into a streambed. *Water Resources Research*, *38*(10), 27–1.
Miles, J. (2014). Tolerance and variance inflation factor. *Wiley statsref: statistics reference online*.
Motta, D., Abad, J. D., & García, M. H. (2010). Modeling framework for organic sediment resuspension and oxygen demand: case of bubbly creek in chicago. *Journal of Environmental Engineering*, *136*(9), 952–964.
Nagaoka, H., & Ohgaki, S. (1990). Mass transfer mechanism in a porous riverbed. *Water Research*, *24*(4), 417–425.
Nikora, V., McLean, S., Coleman, S., Pokrajac, D., McEwan, I., Campbell, L., ... Koll, K. (2007). Double-averaging concept for rough-bed open-channel and overland flows: Applications. *Journal of hydraulic Engineering*, *133*(8), 884–895.
O'Connor, B. L., & Harvey, J. W. (2008). Scaling hyporheic exchange and its influence on biogeochemical reactions in aquatic ecosystems. *Water Resources Research*, *44*(12).
O'Connor, B. L., & Hondzo, M. (2008). Dissolved oxygen transfer to sediments by sweep and eject motions in aquatic environments. *Limnology and Oceanography*, *53*(2), 566–578.
O'Connor, B. L., Hondzo, M., & Harvey, J. W. (2009). Incorporating both physical and kinetic limitations in quantifying dissolved oxygen flux to aquatic sediments. *Journal of Environmental Engineering*, *135*(12), 1304–1314.
OConnor, D. J. (1984). Turbulent transfer across smooth and rough surfaces. In *Gas transfer at water surfaces* (pp. 321–331). Springer.
Packman, A. I., Salehin, M., & Zaramella, M. (2004). Hyporheic exchange with gravel beds: Basic hydrodynamic interactions and bedform-induced advective flows. *Journal of Hydraulic Engineering*, *130*(7), 647–656.
Perry, A. E., Schofield, W. H., & Joubert, P. N. (1969). Rough wall turbulent boundary layers. *Journal of Fluid Mechanics*, *37*(2), 383–413.
Raupach, M., Antonia, R., & Rajagopalan, S. (1991). Rough-wall turbulent boundary layers.
Sakamoto, Y., Ishiguro, M., & Kitagawa, G. (1986). Akaike information criterion statistics. *Dordrecht, The Netherlands: D. Reidel*, *81*(10.5555), 26853.
Shaw, D. A., & Hanratty, T. J. (1977). Turbulent mass transfer rates to a wall for large schmidt numbers. *AIChE Journal*, *23*(1), 28–37.
Steinberger, N., & Hondzo, M. (1999). Diffusional mass transfer at sediment-water interface. *Journal of environmental engineering*, *125*(2), 192–200.
Stoesser, T., Frohlich, J., & Rodi, W. (2007). Turbulent open-channel flow over a permeable bed. In *Proceedings of the congress-international association for hydraulic research* (Vol. 32, p. 189).
Tonina, D., & Buffington, J. M. (2007). Hyporheic exchange in gravel bed rivers with pool-riffle morphology: Laboratory experiments and three-dimensional modeling. *Water Resources Research*, *43*(1).
Voermans, J. J., Ghisalberti, M., & Ivey, G. (2017). The variation of flow and turbulence across the sediment–water interface. *Journal of Fluid Mechanics*, *824*, 413–437.
Voermans, J. J., Ghisalberti, M., & Ivey, G. N. (2018a). The hydrodynamic response of the sediment-water interface to coherent turbulent motions. *Geophysical Research Letters*, *45*(19), 10–520.
Voermans, J. J., Ghisalberti, M., & Ivey, G. N. (2018b). A model for mass transport

across the sediment-water interface. *Water Resources Research*, *54*(4), 2799–2812.

Waterman, D., Liu, X., Motta, D., & García, M. H. (2016). Analytical lagrangian model of sediment oxygen demand and reaeration flux coevolution in streams. *Journal of Environmental Engineering*, *142*(7), 04016028.

Waterman, D., Waratuke, A., Motta, D., Cataño-Lopera, Y., & Garcia, M. H. (2009). Bubbly creek sediment oxygen demand (sod) study with the u of i hydrodynamic sod sampler. *Ven Te Chow Hydrosystems Laboratory, University of Illinois at Urbana–Champaign, Urbana, Ill*.

Waterman, D., Waratuke, A. R., Motta, D., Cataño-Lopera, Y. A., Zhang, H., & García, M. H. (2011). In situ characterization of resuspended-sediment oxygen demand in bubbly creek, chicago, illinois. *Journal of Environmental Engineering*, *137*(8), 717–730.

Wu, H., Zamalloa, C. C. Z., Landry, B. J., & Garcia, M. H. (2019). Experimental comparison of initiation of motion for submerged objects resting on fixed permeable and impermeable beds. *Physical Review Fluids*, *4*(1), 013802.

Supporting Information for "A unifying model for hyporheic oxygen mass transfer under a wide range of near-bed hydrodynamic conditions"

Chieh-Ying Chen[1], Dimitrios K. Fytanidis[2], and Marcelo H. Garcia[3,4]

[1]Graduate Student, Ven Te Chow Hydrosystems Laboratory, Department of Civil and Environmental Engineering, University of Illinois at Urbana-Champaign, 205 North Mathews Ave., Urbana, IL 61801. Email: cyc2@illinois.edu
[2]Adjunct Research Assistant Professor, Ven Te Chow Hydrosystems Laboratory, Department of Civil and Environmental Engineering, University of Illinois at Urbana-Champaign, 205 North Mathews Ave., Urbana, IL 61801. Email: fytanid2@illinois.edu
[3]M.T. Geoffrey Yeh Endowed Chair and Director, Ven Te Chow Hydrosystems Laboratory, Department of Civil and Environmental Engineering, University of Illinois at Urbana-Champaign, 205 North Mathews Ave., Urbana, IL 61801. Email: mhgarcia@illinois.edu
[4]Centro Internacional de Estudios de Grandes Ros, Facultad de Ingeniera y Ciencias Hdricas, Universidad Nacional del Litoral, Santa Fe City, Santa Fe CP 3000, Argentina.

Contents of this file

Corresponding author: Chieh-Ying Chen, cyc2@illinois.edu

SI1: Numerical model verification for result independence

The model using SA-IDDES was validated and compared against Smagorinsky LES model in OpenFOAM by simulating five-layer low-Re case in Manes et al. (2009). Three different mesh resolutions, DES1 with 4.8 million cells, DES1p33 with 12.1 million cells (1.33x finer than DES1) and LES2 with 40.5 million cells (2x finer than DES1), were performed in the domain of $L \times W = 30D \times 15D$ in the depth of $H_w = 1.67D$ and $H_b = 5D$. The boundary conditions are periodic in both streamwise (L) and spanwise (W) directions, non-slip at the bottom of porous media and at spheres, and symmetric at the top of water surface in vertical direction (H). The results were compared with PIV experiment of Manes et al. (2009) and LES simulation of Lian et al. (2021). Figures 1a-d show agreement among experiment, DES and LES models with different mesh resolutions.

In addition to DES/LES and mesh resolutions, we performed detailed analysis to establish result independence considering domain size and integration time. Four different domain sizes, $L \times W$=$18D \times 9D$ (2.5 million cells), $36D \times 18D$ (10.1 million cells), $72D\times36D$ (40.5 million cells), and $90D\times36D$ (50.6 million cells) in the depth of $H_w = 13.38D$ and $H_b = 4.46D$ with the same mesh resolution, were tested to ensure the modeling domain is large enough to apply periodic boundary conditions. The statistics for turbulence quantities become consistent when the domain is larger than $36D\times18D$ (Figures 1e-g), which is considered as the most cost-effective size and this simulation domain is selected in the current study.

Double-averaging method is used to study the turbulence statistics while using periodic boundary conditions. To ensure the simulation time is sufficiently long to construct the representative vertical profile, the analysis of integration time is performed to determine appropriate simulation flow cycles. Two simulation time, 167 and 234 flow cycles, were performed and they both show good convergence in Figures 1h-j. Therefore, running the simulation for at least 200 flow cycles is considered reliable for turbulence statistics while using periodic boundary conditions and double-averaging method.

SI2: Numerical setup and parameter selection for all simulation cases

Table 1 summarizes all cases that have been examined in the present study, aiming to expand the existing dataset for high Reynolds number and bed roughness.

SI3: Collection of D_{eff}/D_m dataset for model foundation

Table 3 integrates field and flume data from earlier studies (O'Connor & Harvey, 2008; Grant et al., 2012; Voermans et al., 2018) along with our numerical results. The dataset combines 93 field and flume samples and 17 simulations in current study.

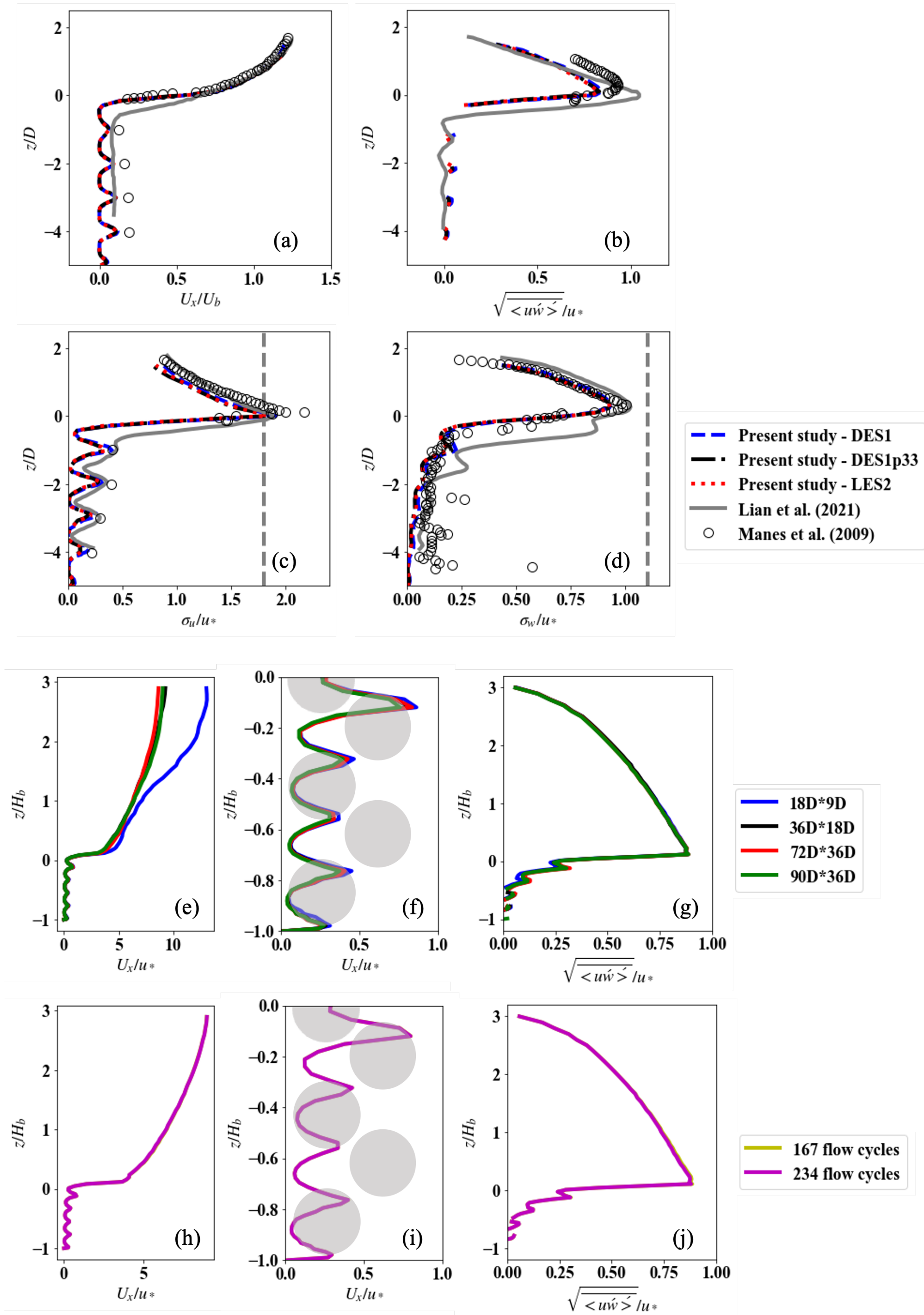

Figure 1. (a), (b), (c) and (d) Model validation of DES/LES and mesh resolutions for U_x/U_b, $\sqrt{<\overline{u'w'}>}/u_*$, σ_u/u_* and σ_w/u_*. (e), (f) and (g) justification of domain size for U_x/u_* and $\sqrt{<\overline{u'w'}>}/u_*$. (h), (i) and (j) justification of integration time.

Table 1. Parameter selection of total 14 simulations.

Case name (Symbol)	Bed type	ϕ	H_w (m)	H_b (m)	U_b (m/s)	u_* (m/s)	K (m^2)	Re_*	Re_k
Base case ●	impermeable	N/A	0.134	N/A	1	0.093	N/A	2326.84	N/A
	hyporheic	0.6	0.134	0.045	1	0.168	7.5×10^{-7}	4208.44	145.79
Low Re ●	impermeable	N/A	0.134	N/A	0.1	0.008	N/A	192.06	N/A
	hyporheic	0.6	0.134	0.045	0.1	0.013	7.5×10^{-7}	319.60	11.07
Moderate Re ●	impermeable	N/A	0.134	N/A	0.5	0.045	N/A	1119.01	N/A
	hyporheic	0.6	0.134	0.045	0.5	0.074	7.5×10^{-7}	1839.88	63.74
High Re ●	impermeable	N/A	0.134	N/A	10	1.036	N/A	25896.83	N/A
	hyporheic	0.6	0.134	0.045	10	2.006	7.5×10^{-7}	50137.81	1736.83
Compact ▲	impermeable	N/A	0.107	N/A	1	0.099	N/A	2485.13	N/A
	hyporheic	0.4	0.107	0.036	1	0.131	9.877×10^{-8}	3276.29	41.19
Shallow ■	impermeable	N/A	0.045	N/A	1	0.123	N/A	3063.98	N/A
	hyporheic	0.6	0.045	0.045	1	0.345	7.5×10^{-7}	8624.99	298.78
Deep ■	impermeable	N/A	0.312	N/A	1	0.069	N/A	1724.24	N/A
	hyporheic	0.6	0.312	0.045	1	0.097	7.5×10^{-7}	2425.96	84.04

* Particle diameter (D) is 0.01 m and roughness height ($k_s = 2.5D$) is 0.025 m (Engelund, 1970; Garcia, 2008) for all cases.

** Permeability (K) is computed by the KozenyCarman model : $K = \frac{\phi^3 d^2}{180(1-\phi)^2}$ (p. 166 in Bear (1972).

*** All cases are simulated as incompressible and isothermal with $\nu = 1 \times 10^{-6}$ m^2/s at 20 $^\circ C$.

Table 2: Collection of parameters in previously published dataset and current study.

Source, Tracer	Exp.	Bed form	U (m/s)	u_* (m/s)	k_s (m)	K (m^2)	ν (m^2/s)	H_w (m)	H_b (m)	ϕ
Richardson and Parr (1988), Fluorescein	a6	Plane	0.0366	0.0033	0.00948	7.14E-09	1.53E-06	0.013	0.0254	0.38
	d1	Plane	0.0762	0.00552	0.00314	7.91E-10	9.78E-07	0.00635	0.0254	0.4
	d1r	Plane	0.0792	0.00752	0.00314	7.91E-10	9.77E-07	0.00635	0.0254	0.4
	d2	Plane	0.0366	0.00271	0.00314	7.91E-10	1.06E-06	0.013	0.0254	0.4
	d3	Plane	0.152	0.0108	0.00314	7.91E-10	1.07E-06	0.013	0.0254	0.4
	b1	Plane	0.226	0.0129	0.00154	1.58E-10	1.09E-06	0.0135	0.0254	0.38
	b2	Plane	0.155	0.00936	0.00154	1.58E-10	1.05E-06	0.0127	0.0254	0.38
	b2r	Plane	0.152	0.0112	0.00154	1.58E-10	1.16E-06	0.0124	0.0254	0.38
	b5	Plane	0.0792	0.00524	0.00154	1.58E-10	1.01E-06	0.0066	0.0254	0.38
	b5r	Plane	0.0762	0.00808	0.00154	1.58E-10	1.12E-06	0.0066	0.0254	0.38
	b6	Plane	0.0366	0.00268	0.00154	1.58E-10	1.09E-06	0.0127	0.0254	0.38
	b7	Plane	0.152	0.00885	0.00154	1.58E-10	1.09E-06	0.0188	0.0254	0.38
	b8	Plane	0.0701	0.00443	0.00154	1.58E-10	1.09E-06	0.0188	0.0254	0.38
	b8r	Plane	0.0762	0.00602	0.00154	1.58E-10	1.26E-06	0.0193	0.0254	0.38
	e1	Plane	0.0792	0.00524	0.000888	5.43E-11	9.69E-07	0.0066	0.0254	0.37
	e1r	Plane	0.0762	0.00762	0.000888	5.43E-11	9.49E-07	0.0066	0.0254	0.37
	e2	Plane	0.155	0.00869	0.000888	5.43E-11	1.04E-06	0.0127	0.0254	0.37
	e2r	Plane	0.152	0.0116	0.000888	5.43E-11	1.01E-06	0.0124	0.0254	0.37
	e3	Plane	0.0366	0.00265	0.000888	5.43E-11	1.04E-06	0.013	0.0254	0.37
	e4	Plane	0.229	0.0117	0.000888	5.43E-11	1.02E-06	0.013	0.0254	0.37
	c1	Plane	0.152	0.0104	0.00033	1.7E-11	1.36E-06	0.0127	0.0254	0.36
	c1r	Plane	0.152	N/A	0.00033	1.7E-11	1.03E-06	0.0127	0.0254	0.36
	c2	Plane	0.0762	0.00703	0.00033	1.7E-11	1.34E-06	0.0066	0.0254	0.36
	c2r	Plane	0.0732	0.01	0.00033	1.7E-11	1.36E-06	0.00686	0.0254	0.36
	c3	Plane	0.0366	0.00361	0.00033	1.7E-11	1.44E-06	0.013	0.0254	0.36
Elliot and Brooks (1977), NaCl	8	Bed form	0.132	0.0159	0.00946	1.12E-10	1.00E-06	0.0645	0.13	0.33
	9	Bed form	0.132	0.0244	0.0289	1.12E-10	1.00E-06	0.0645	0.135	0.33
	10	Bed form	0.087	0.0154	0.0154	1.12E-10	1.00E-06	0.031	0.126	0.33
	12	Bed form	0.132	0.0195	0.0154	1.12E-10	1.00E-06	0.0648	0.125	0.33

	14	Bed form	0.086	0.0129	0.0154	1.12E-10	1.00E-06	0.0648	0.22	0.33
	15	Bed form	0.087	0.0143	0.0289	1.12E-10	1.00E-06	0.0648	0.22	0.33
	16	Bed form	0.107	0.0171	0.0197	1.12E-10	1.00E-06	0.0648	0.22	0.33
	17	Bed form	0.087	0.014	0.0129	8.05E-12	1.00E-06	0.0645	0.225	0.3
Packman et al. (2000), LiCl	7	Bed form	0.152	0.0158	0.0121	1.53E-10	1.00E-06	0.127	0.119	0.33
	13	Bed form	0.144	0.0155	0.0118	1.53E-10	1.00E-06	0.09	0.1	0.33
	15	Bed form	0.126	0.0152	0.015	1.53E-10	1.00E-06	0.079	0.097	0.33
Marion et al. (2002), NaCl	S1	Plane	0.25	0.0172	0.00338	5.04E-10	1.30E-06	0.109	0.4	0.38
	S2	Ripples	0.24	0.0173	0.0054	5.04E-10	1.30E-06	0.11	0.4	0.38
	S3	Dunes/Ripples	0.28	0.0182	0.00849	5.04E-10	1.30E-06	0.118	0.4	0.38
	S4	Dunes	0.22	0.0176	0.0236	5.04E-10	1.30E-06	0.123	0.4	0.38
	S5	Dunes	0.22	0.0177	0.018	5.04E-10	1.30E-06	0.121	0.4	0.38
Packman and McCay (2003), NaCl	1	Dunes	0.233	0.0171	0.0166	1.83E-10	1.00E-06	0.087	0.099	0.38
	2a	Dunes	0.237	0.0153	0.0172	1.83E-10	1.00E-06	0.118	0.099	0.38
	2b	Dunes	0.237	0.0153	0.0172	6.8E-11	1.00E-06	0.118	0.099	0.29
	3a	Dunes	0.236	0.017	0.0159	1.83E-10	1.00E-06	0.086	0.103	0.38
	3b	Dunes	0.236	0.017	0.0159	6.8E-11	1.00E-06	0.086	0.103	0.29
Rehg et al. (2005), NaCl	1	Natural bed	0.154	0.0066	0.0132	1.82E-10	1.00E-06	0.109	0.105	0.36
	2	Natural bed	0.164	0.0146	0.0158	1.82E-10	1.00E-06	0.104	0.0986	0.36
Tonina and Buffington (2007), Fluorescein	1	Pool-riffle	0.282	0.0511	0.116	5.1E-09	1.00E-06	0.065	0.18	0.34
	2	Pool-riffle	0.384	0.0549	0.116	5.1E-09	1.00E-06	0.075	0.18	0.34
	3	Pool-riffle	0.369	0.0429	0.116	5.1E-09	1.00E-06	0.104	0.18	0.34
	4	Pool-riffle	0.308	0.0475	0.094	5.1E-09	1.00E-06	0.056	0.18	0.34
	5	Pool-riffle	0.413	0.0507	0.094	5.1E-09	1.00E-06	0.064	0.18	0.34
	6	Pool-riffle	0.421	0.0392	0.094	5.1E-09	1.00E-06	0.087	0.18	0.34
	7	Pool-riffle	0.365	0.0421	0.0792	5.1E-09	1.00E-06	0.044	0.18	0.34
	8	Pool-riffle	0.46	0.0462	0.0792	5.1E-09	1.00E-06	0.053	0.18	0.34
	9	Pool-riffle	0.425	0.039	0.0792	5.1E-09	1.00E-06	0.086	0.18	0.34
	10	Pool-riffle	0.367	0.0396	0.064	5.1E-09	1.00E-06	0.039	0.18	0.34
	11	Pool-riffle	0.452	0.0457	0.064	5.1E-09	1.00E-06	0.052	0.18	0.34
	12	Pool-riffle	0.442	0.0381	0.064	5.1E-09	1.00E-06	0.082	0.18	0.34
Nagaoka and Ohgaki (1990), NaCl	1	Plane	0.428	0.043	0.245	2.31E-07	1.00E-06	0.0675	0.236	0.24
	2	Plane	0.28	0.0407	0.245	2.31E-07	1.00E-06	0.0675	0.236	0.24

	3	Plane	0.211	0.027	0.245	2.31E-07	1.00E-06	0.0675	0.236	0.24
	4	Plane	0.167	0.0218	0.245	2.31E-07	1.00E-06	0.0675	0.236	0.24
	5	Plane	0.117	0.0153	0.245	2.31E-07	1.00E-06	0.07	0.236	0.24
	6	Plane	0.089	0.0115	0.245	2.31E-07	1.00E-06	0.0675	0.236	0.24
	10	Plane	0.302	0.0291	0.114	5.02E-08	1.00E-06	0.032	0.115	0.24
	11	Plane	0.203	0.0165	0.114	5.02E-08	1.00E-06	0.032	0.115	0.24
	12	Plane	0.112	0.0109	0.114	5.02E-08	1.00E-06	0.032	0.115	0.24
Ren and Packman (2004), NaCl	2	Bed form	0.13	0.00482	0.0131	1.82E-10	1.00E-06	0.079	0.0924	0.36
	3	Bed	0.144	0.00456	0.0114	1.82E-10	1.00E-06	0.0707	0.104	0.36
	4	Bed	0.141	0.00464	0.00905	1.82E-10	1.00E-06	0.073	0.102	0.36
	5	Bed	0.12	0.00505	0.00957	1.82E-10	1.00E-06	0.0865	0.114	0.36
	6	Bed	0.157	0.00515	0.00909	1.82E-10	1.00E-06	0.09	0.113	0.36
Lai et al. (1994), KCl	a6	Plane	0.154	0.00597	0.0207	1.86E-09	1.00E-06	0.0097	0.15	0.38
	a8	Plane	0.0741	0.00236	0.0207	1.86E-09	1.00E-06	0.0202	0.15	0.38
	a9	Plane	0.101	0.00342	0.0207	1.86E-09	1.00E-06	0.0199	0.15	0.38
	b1	Plane	0.0988	0.00338	0.0125	1.29E-09	1.00E-06	0.0051	0.15	0.38
	b4	Plane	0.0988	0.00359	0.0125	1.29E-09	1.00E-06	0.0101	0.15	0.38
	b7	Plane	0.0998	0.00347	0.0125	1.29E-09	1.00E-06	0.015	0.15	0.38
	c4	Plane	0.0998	0.00471	0.00701	6.1E-10	1.00E-06	0.005	0.15	0.37
	d4	Plane	0.101	0.00468	0.00354	2.31E-10	1.00E-06	0.0049	0.15	0.36
Packman et al. (2004), NaCl	1	Plane	0.361	0.0319	0.0526	1.53E-08	1.00E-06	0.114	0.19	0.38
	2	Plane	0.274	0.0275	0.0526	1.53E-08	1.00E-06	0.113	0.19	0.38
	3	Plane	0.179	0.0198	0.0526	1.53E-08	1.00E-06	0.114	0.19	0.38
	4	Plane	0.091	0.0106	0.0526	1.53E-08	1.00E-06	0.114	0.19	0.38
	5	Plane	0.179	0.0301	0.0526	1.53E-08	1.00E-06	0.201	0.19	0.38
	6	Plane	0.092	0.0167	0.0526	1.53E-08	1.00E-06	0.202	0.19	0.38
	7	Bed form	0.177	0.0279	0.0648	1.53E-08	1.00E-06	0.204	0.19	0.38
	8	Bed form	0.09	0.0276	0.0648	1.53E-08	1.00E-06	0.205	0.19	0.38
	9	Bed form	0.268	0.0283	0.0462	1.53E-08	1.00E-06	0.204	0.19	0.38
	10	Bed form	0.177	0.015	0.0462	1.53E-08	1.00E-06	0.203	0.19	0.38
	11	Bed form	0.091	0.0237	0.0462	1.53E-08	1.00E-06	0.204	0.19	0.38
Present study, numerical modeling	Base	Hyporheic	1.000	0.1683	0.025	7.5E-07	1.00E-06	0.134	0.045	0.6
	Low Re	Hyporheic	0.100	0.0128	0.025	7.5E-07	1.00E-06	0.134	0.045	0.6

	Moderate Re	Hyporheic	0.500	0.0736	0.025	7.5E-07	1.00E-06	0.134	0.045	0.6
	High Re	Hyporheic	10.000	2.0055	0.025	7.5E-07	1.00E-06	0.134	0.045	0.6
	Compact	Hyporheic	1.000	0.1311	0.025	9.88E-08	1.00E-06	0.107	0.036	0.4
	Shallow	Hyporheic	1.000	0.3450	0.025	7.5E-07	1.00E-06	0.045	0.045	0.6
	Deep	Hyporheic	1.000	0.0970	0.025	7.5E-07	1.00E-06	0.312	0.045	0.6
	Base	Impermeable	1.000	0.0931	0.025	N/A	1.00E-06	0.134	0.000	0.6
	Low Re	Impermeable	0.100	0.0077	0.025	N/A	1.00E-06	0.134	0.000	0.6
	Moderate Re	Impermeable	0.500	0.0448	0.025	N/A	1.00E-06	0.134	0.000	0.6
	High Re	Impermeable	10.000	1.0359	0.025	N/A	1.00E-06	0.134	0.000	0.6
	Compact	Impermeable	1.000	0.0994	0.025	N/A	1.00E-06	0.107	0.000	0.4
	Shallow	Impermeable	1.000	0.1226	0.025	N/A	1.00E-06	0.045	0.000	0.6
	Deep	Impermeable	1.000	0.0690	0.025	N/A	1.00E-06	0.312	0.000	0.6
	BM-DES1	Hyporheic	0.252	0.0306	0.03	3.16E-07	1.00E-06	0.026	0.054	0.48
	BM-DES1p33	Hyporheic	0.252	0.0294	0.03	3.16E-07	1.00E-06	0.026	0.054	0.48
	BM-LES2	Hyporheic	0.254	0.0306	0.03	3.16E-07	1.00E-06	0.026	0.054	0.48

Table 3: Collection of Reynolds and Peclet numbers in previously published dataset and current study.

Exp. .	Bed form	$D_m(m^2/s)$	$D_{eff}(m^2/s)$	$\frac{Deff}{D_m}$	$Re_{bulk} = \frac{U_b H_w}{\nu}$	$Re_{H_w} = \frac{u_* H_w}{\nu}$	$Re_{H_b} = \frac{u_* H_b}{\nu}$	$Pe_k = \frac{u_* \sqrt{K}}{D_m}$	$Re_k = \frac{u_* \sqrt{K}}{\nu}$	$Re_* = \frac{u_* k_s}{\nu}$
a6	Plane	4.75E-10	2.17E-08	45.60	310.00	27.90	54.80	586.04	0.18	20.40
d1	Plane	4.75E-10	1.83E-08	38.50	495.00	35.90	143.00	327.54	0.16	17.70
d1r	Plane	4.75E-10	5.43E-08	114.00	515.00	48.90	195.00	444.96	0.22	24.10
d2	Plane	4.75E-10	2.10E-09	4.42	445.00	33.00	64.70	160.38	0.07	7.99
d3	Plane	4.75E-10	3.93E-08	82.70	1850.00	131.00	256.00	639.00	0.28	31.70
b1	Plane	4.75E-10	4.80E-08	101.00	2800.00	159.00	301.00	341.21	0.15	18.20
b2	Plane	4.75E-10	1.81E-08	38.20	1880.00	113.00	226.00	248.64	0.11	13.70
b2r	Plane	4.75E-10	4.93E-08	104.00	1640.00	120.00	245.00	295.24	0.12	14.80
b5	Plane	4.75E-10	3.81E-09	8.01	520.00	34.40	132.00	138.86	0.07	8.00
b5r	Plane	4.75E-10	1.52E-08	32.10	450.00	47.70	184.00	213.38	0.09	11.10
b6	Plane	4.75E-10	1.22E-09	2.57	425.00	31.20	62.30	70.84	0.03	3.77
b7	Plane	4.75E-10	2.55E-08	53.70	2630.00	152.00	206.00	234.60	0.10	12.50
b8	Plane	4.75E-10	3.23E-09	6.79	1210.00	76.50	103.00	117.25	0.05	6.25
b8r	Plane	4.75E-10	5.75E-09	12.10	1170.00	92.50	122.00	159.53	0.06	7.36
e1	Plane	4.75E-10	9.13E-10	1.92	540.00	35.70	137.00	81.19	0.04	4.80
e1r	Plane	4.75E-10	4.44E-09	9.36	530.00	53.00	204.00	118.20	0.06	7.13
e2	Plane	4.75E-10	3.38E-09	7.12	1900.00	106.00	212.00	134.47	0.06	7.41
e2r	Plane	4.75E-10	1.22E-08	25.70	1870.00	142.00	289.00	179.55	0.08	10.10
e3	Plane	4.75E-10	4.30E-10	0.91	455.00	33.00	64.60	40.95	0.02	2.26
e4	Plane	4.75E-10	1.11E-08	23.30	2900.00	149.00	291.00	181.68	0.08	10.20
c1	Plane	4.75E-10	2.21E-09	4.65	1420.00	96.60	193.00	90.12	0.03	2.51
c1r	Plane	4.75E-10	2.56E-09	5.38	1880.00	N/A	N/A	N/A	N/A	N/A
c2	Plane	4.75E-10	5.21E-10	1.10	375.00	34.60	133.00	61.13	0.02	1.73
c2r	Plane	4.75E-10	1.12E-09	2.36	370.00	50.70	188.00	86.93	0.03	2.44
c3	Plane	4.75E-10	2.59E-10	0.55	330.00	32.60	63.90	31.41	0.01	0.83
8	Bed form	4.10E-10	2.20E-07	536.00	8510.00	1030.00	2070.00	409.92	0.17	151.00
9	Bed form	4.10E-10	1.95E-07	476.00	8510.00	1570.00	3290.00	629.52	0.26	705.00

10	Bed form	4.10E-10	3.29E-08	80.30	2700.00	477.00	1940.00	397.72	0.16	237.00
12	Bed form	4.10E-10	1.08E-07	264.00	8550.00	1270.00	2440.00	505.08	0.21	300.00
14	Bed form	4.10E-10	3.93E-08	95.90	5570.00	833.00	2830.00	331.84	0.14	198.00
15	Bed form	4.10E-10	1.03E-07	250.00	5640.00	924.00	3140.00	368.44	0.15	413.00
16	Bed form	4.10E-10	2.50E-07	610.00	6930.00	1110.00	3760.00	441.64	0.18	336.00
17	Bed form	4.10E-10	1.05E-08	25.60	5610.00	903.00	3150.00	96.87	0.04	180.00
7	Bed form	8.70E-10	1.54E-07	177.00	19300.00	2000.00	1880.00	224.25	0.20	191.00
13	Bed form	8.70E-10	1.28E-07	147.00	13000.00	1400.00	1550.00	220.80	0.19	184.00
15	Bed form	8.70E-10	1.33E-07	153.00	9950.00	1200.00	1480.00	217.35	0.19	229.00
S1	Plane	1.50E-09	1.16E-06	776.00	21000.00	1440.00	5290.00	257.50	0.30	44.60
S2	Ripples	1.50E-09	2.21E-06	1480.00	20200.00	1460.00	5320.00	258.37	0.30	71.80
S3	Dunes/Ripples	1.50E-09	2.61E-06	1740.00	25300.00	1640.00	5600.00	272.24	0.31	119.00
S4	Dunes	1.50E-09	4.06E-06	2710.00	20800.00	1670.00	5410.00	263.57	0.30	319.00
S5	Dunes	1.50E-09	6.78E-06	4520.00	20500.00	1650.00	5460.00	265.30	0.31	246.00
1	Dunes	1.50E-09	6.49E-07	433.00	20300.00	1490.00	1690.00	154.74	0.23	283.00
2a	Dunes	1.50E-09	2.50E-07	167.00	28000.00	1810.00	1510.00	138.07	0.21	263.00
2b	Dunes	1.50E-09	2.49E-07	166.00	28000.00	1810.00	1510.00	84.04	0.13	263.00
3a	Dunes	1.50E-09	1.25E-07	83.40	20300.00	1460.00	1750.00	153.41	0.23	270.00
3b	Dunes	1.50E-09	1.30E-07	86.40	20300.00	1460.00	1750.00	93.38	0.14	270.00
1	Natural bed	1.50E-09	6.12E-08	40.80	16700.00	717.00	696.00	59.36	0.09	87.30
2	Natural bed	1.50E-09	1.97E-07	131.00	17100.00	1520.00	1440.00	131.40	0.20	231.00
1	Pool-riffle	4.75E-10	5.10E-05	107000.00	18300.00	3320.00	9200.00	7701.50	3.65	5920.00
2	Pool-riffle	4.75E-10	3.64E-05	76600.00	28800.00	4120.00	9890.00	8271.20	3.92	6360.00
3	Pool-riffle	4.75E-10	4.09E-05	86200.00	38400.00	4460.00	7710.00	6456.60	3.06	4960.00
4	Pool-riffle	4.75E-10	4.61E-05	97100.00	17200.00	2660.00	8540.00	7152.90	3.39	4460.00
5	Pool-riffle	4.75E-10	1.38E-04	291000.00	26400.00	3250.00	9130.00	7638.20	3.62	4770.00
6	Pool-riffle	4.75E-10	6.62E-05	139000.00	36600.00	3410.00	7060.00	5908.00	2.80	3680.00
7	Pool-riffle	4.75E-10	7.23E-05	152000.00	16100.00	1850.00	7570.00	6330.00	3.00	3330.00
8	Pool-riffle	4.75E-10	5.30E-05	112000.00	24400.00	2450.00	8310.00	6963.00	3.30	3660.00
9	Pool-riffle	4.75E-10	3.90E-05	82200.00	36600.00	3350.00	7010.00	5865.80	2.78	3090.00
10	Pool-riffle	4.75E-10	3.69E-05	77600.00	14300.00	1540.00	7130.00	5971.30	2.83	2530.00
11	Pool-riffle	4.75E-10	3.50E-05	73800.00	23500.00	2380.00	8230.00	6878.60	3.26	2930.00

12	Pool-riffle	4.75E-10	2.18E-05	45900.00	36200.00	3120.00	6850.00	5739.20	2.72	2440.00
1	Plane	1.50E-09	6.46E-04	430000.00	28900.00	2900.00	10100.00	13806.90	20.70	10500.00
2	Plane	1.50E-09	4.33E-04	289000.00	18900.00	2750.00	9610.00	13073.20	19.60	9960.00
3	Plane	1.50E-09	1.55E-04	103000.00	14200.00	1820.00	6370.00	8671.00	13.00	6610.00
4	Plane	1.50E-09	1.26E-04	83800.00	11300.00	1470.00	5140.00	7003.50	10.50	5340.00
5	Plane	1.50E-09	9.09E-05	60600.00	8190.00	1070.00	3610.00	4909.12	7.36	3750.00
6	Plane	1.50E-09	6.58E-05	43900.00	6010.00	776.00	2710.00	3688.51	5.53	2820.00
10	Plane	1.50E-09	1.51E-04	100000.00	9660.00	931.00	3350.00	4348.84	6.52	3320.00
11	Plane	1.50E-09	7.62E-05	50800.00	6500.00	528.00	1900.00	2467.90	3.70	1880.00
12	Plane	1.50E-09	1.88E-05	12500.00	3580.00	349.00	1250.00	1627.48	2.44	1240.00
2	Bed form	1.50E-09	2.44E-08	16.20	10300.00	381.00	446.00	43.36	0.07	63.00
3	Bed	1.50E-09	5.94E-08	39.60	10200.00	322.00	473.00	41.02	0.06	52.10
4	Bed	1.50E-09	3.72E-08	24.80	10300.00	338.00	475.00	41.69	0.06	41.90
5	Bed	1.50E-09	8.30E-08	55.30	10300.00	436.00	574.00	45.42	0.07	48.30
6	Bed	1.50E-09	1.52E-07	101.00	14100.00	463.00	583.00	46.29	0.07	46.80
a6	Plane	1.50E-09	5.94E-07	396.00	1490.00	57.90	895.00	171.42	0.26	123.00
a8	Plane	1.50E-09	2.14E-08	14.30	1500.00	47.60	353.00	68.03	0.10	48.70
a9	Plane	1.50E-09	5.65E-08	37.70	2010.00	68.10	513.00	98.72	0.15	70.80
b1	Plane	1.50E-09	1.71E-07	114.00	504.00	17.20	507.00	80.71	0.12	42.20
b4	Plane	1.50E-09	4.46E-08	29.70	998.00	36.20	538.00	86.04	0.13	44.80
b7	Plane	1.50E-09	2.20E-08	14.60	1500.00	52.10	521.00	83.38	0.13	43.40
c4	Plane	1.50E-09	9.61E-08	64.10	499.00	23.50	706.00	77.37	0.12	33.00
d4	Plane	1.50E-09	2.73E-08	18.20	495.00	22.90	702.00	47.49	0.07	16.60
1	Plane	1.50E-09	1.58E-04	106000.00	41200.00	3640.00	6060.00	2627.98	3.94	1680.00
2	Plane	1.50E-09	1.06E-04	70600.00	31000.00	3100.00	5220.00	2261.13	3.39	1450.00
3	Plane	1.50E-09	4.60E-05	30700.00	20400.00	2260.00	3760.00	1634.15	2.45	1040.00
4	Plane	1.50E-09	7.08E-06	4720.00	10400.00	1210.00	2010.00	873.77	1.31	557.00
5	Plane	1.50E-09	1.22E-04	81500.00	36000.00	6050.00	5720.00	2481.24	3.72	1590.00
6	Plane	1.50E-09	2.05E-05	13700.00	18600.00	3360.00	3160.00	1374.02	2.06	877.00
7	Bed form	1.50E-09	1.83E-04	122000.00	36100.00	5700.00	5310.00	2301.15	3.45	1810.00
8	Bed form	1.50E-09	4.85E-05	32300.00	18500.00	5670.00	5250.00	2281.14	3.42	1790.00
9	Bed form	1.50E-09	2.73E-04	182000.00	54700.00	5770.00	5380.00	2334.50	3.50	1310.00
10	Bed form	1.50E-09	1.83E-04	122000.00	35900.00	3050.00	2850.00	1233.95	1.85	693.00

11	Bed form	1.50E-09	4.85E-05	32300.00	18600.00	4830.00	4500.00	1954.31	2.93	1090.00
Base	Hyporheic	2.00E-09	8.33E-04	416509.55	133791.00	22522.07	7507.36	72892.37	145.78	4208.44
Low Re	Hyporheic	2.00E-09	4.39E-05	21956.53	13379.10	1710.39	570.13	5535.67	11.07	319.60
Moderate Re	Hyporheic	2.00E-09	3.52E-04	176040.39	66895.50	9846.36	3282.12	31867.60	63.74	1839.88
High Re	Hyporheic	2.00E-09	9.88E-03	4941608.87	1337910.00	268319.53	89439.84	868412.42	1736.82	50137.81
Compact	Hyporheic	2.00E-09	8.87E-04	443437.23	106800.00	13996.32	4665.44	20592.78	41.19	3276.29
Shallow	Hyporheic	2.00E-09	1.52E-03	757797.07	44597.00	15385.95	15385.95	149389.23	298.78	8624.99
Deep	Hyporheic	2.00E-09	3.49E-04	174575.94	312179.00	30293.41	4327.63	42018.94	84.04	2425.96
Base	Impermeable	2.00E-09	3.07E-04	153536.98	133791.00	12452.40	N/A	N/A	N/A	2326.84
Low Re	Impermeable	2.00E-09	1.42E-05	7088.30	13379.10	1027.84	N/A	N/A	N/A	192.06
Moderate Re	Impermeable	2.00E-09	1.38E-04	68859.41	66895.50	5988.55	N/A	N/A	N/A	1119.01
High Re	Impermeable	2.00E-09	3.58E-03	1789636.17	1337910.00	138590.50	N/A	N/A	N/A	25896.83
Compact	Impermeable	2.00E-09	6.34E-04	317234.17	106800.00	10616.46	N/A	N/A	N/A	2485.13
Shallow	Impermeable	2.00E-09	2.68E-04	133751.71	44597.00	5465.77	N/A	N/A	N/A	3063.98
Deep	Impermeable	2.00E-09	1.58E-04	79122.89	312179.00	21530.87	N/A	N/A	N/A	1724.24
BM-DES1	Hyporheic	2.00E-09	7.60E-05	38003.00	6564.95	796.68	1654.64	8605.62	17.21	919.24
BM-DES1p33	Hyporheic	2.00E-09	6.83E-05	34171.33	6546.85	764.10	1586.97	8253.68	16.51	881.65
BM-LES2	Hyporheic	2.00E-09	7.23E-05	36142.85	6598.29	795.78	1652.77	8595.90	17.19	918.20

Table 4. Five best models of D_{eff}/D_m fitness in MLR analysis

Model	R^2	AIC	VIF
$\frac{D_{eff}}{D_m} = Re_k^{1.08} Re_{H_b}^{1.04}$	0.984	127	1.00
$\frac{D_{eff}}{D_m} = Re_*^{1.31} Re_k^{0.39}$	0.98	149	1.03
$\frac{D_{eff}}{D_m} = Re_{bulk}^{0.85} Re_k^{1.15}$	0.974	178	1.00
$\frac{D_{eff}}{D_m} = Re_k^{1.71} \phi^{-7.59}$	0.969	195	1.06
$\frac{D_{eff}}{D_m} = Re_{Hw}^{1.13} Re_k^{0.86}$	0.968	198	1.00

SI4: Five best models of D_{eff}/D_m fitness in MLR analysis

Table 4 summarizes the 5 models with best fitness to the training data of D_{eff}/D_m (Table 4).

SI5: Collection of $\tilde{K_L}$ dataset for model foundation

Table 5 integrates dataset reported by O'Connor et al. (2009), Han et al. (2018) and Voermans et al. (2018). The dataset that includes smooth to fully rough beds and low to high permeabilities for mass transfer coefficient (Steinberger & Hondzo, 1999; O'Connor & Hondzo, 2008; O'Connor et al., 2009; Nagaoka & Ohgaki, 1990; Elliott & Brooks, 1997; Marion et al., 2002; Packman et al., 2004; Tonina & Buffington, 2007; Voermans et al., 2017).

Table 5: Collection of mass transfer coefficients in previously published dataset and current study

Source	Exp.	u_* (m/s)	D (m)	K (m^2)	Re_k	Re_*	$\tilde{K}_L$ (m/s)
O'Connor et al. (2009)	Thin-film theory	0.0797	0.00004	1.200E-11	0.276	7.974	4.001E-05
	(diffusive sublayer thickness)	0.1614	0.00004	1.200E-11	0.559	16.135	1.070E-04
		0.2013	0.00004	1.200E-11	0.697	20.130	7.979E-05
		0.2222	0.00004	1.200E-11	0.770	22.216	1.067E-04
		0.2295	0.00004	1.200E-11	0.795	22.949	2.865E-04
		0.3092	0.00004	1.200E-11	1.071	30.922	3.355E-04
		0.4383	0.00004	1.200E-11	1.518	43.830	4.247E-04
		0.3905	0.00004	1.200E-11	1.353	39.047	6.363E-04
		0.5279	0.00004	1.200E-11	1.829	52.792	1.476E-03
		0.5581	0.00004	1.200E-11	1.933	55.807	1.643E-03
		0.4580	0.00004	1.200E-11	1.587	45.800	1.216E-03
	Thin-film theory	0.0774	0.00004	1.200E-11	0.268	7.745	3.008E-04
	(Batchelor length)	0.1588	0.00004	1.200E-11	0.550	15.879	5.432E-04
		0.2006	0.00004	1.200E-11	0.695	20.059	5.474E-04
		0.2193	0.00004	1.200E-11	0.760	21.927	7.587E-04
		0.2306	0.00004	1.200E-11	0.799	23.062	7.901E-04
		0.3082	0.00004	1.200E-11	1.068	30.824	9.830E-04
		0.3880	0.00004	1.200E-11	1.344	38.801	1.010E-03
		0.4580	0.00004	1.200E-11	1.587	45.802	1.202E-03
		0.4368	0.00004	1.200E-11	1.513	43.685	1.382E-03
		0.5262	0.00004	1.200E-11	1.823	52.616	1.382E-03
		0.5584	0.00004	1.200E-11	1.934	55.836	1.449E-03
	Surface renewal theory	0.0813	0.00004	1.200E-11	0.282	8.133	2.468E-04
		0.1589	0.00004	1.200E-11	0.550	15.887	4.892E-04
		0.1987	0.00004	1.200E-11	0.688	19.872	5.250E-04
		0.2155	0.00004	1.200E-11	0.747	21.552	7.227E-04
		0.2269	0.00004	1.200E-11	0.786	22.687	7.586E-04
		0.3063	0.00004	1.200E-11	1.061	30.634	9.830E-04
		0.3860	0.00004	1.200E-11	1.337	38.600	1.077E-03

		0.4367	0.00004	1.200E-11	1.513	43.670	1.477E-03
		0.4577	0.00004	1.200E-11	1.586	45.775	1.382E-03
		0.5278	0.00004	1.200E-11	1.828	52.775	1.584E-03
		0.5561	0.00004	1.200E-11	1.926	55.612	1.670E-03
Han et al. (2018)	Nagaoka and Ohgaki (1990)	0.0109	0.019	1.420E-07	4.107	207.100	1.014E-03
(Rough-bed dataset)		0.0407	0.041	1.080E-06	42.297	1660.600	1.123E-02
	Elliott and Brooks (1997)	0.0131	0.00012	8.480E-12	0.038	6.100	1.009E-04
		0.0247	0.00046	1.180E-10	0.268	11.500	1.075E-03
	Marion et al. (2002)	0.0173	0.0008	5.000E-10	0.387	13.900	1.972E-04
		0.0183	0.0008	5.000E-10	0.409	14.700	1.157E-03
	Packman et al. (2004)	0.0166	0.0049	4.690E-11	0.114	82.000	6.640E-04
		0.0319	0.005	1.560E-10	0.398	160.000	4.785E-03
	Tonina and Buffington (2007)	0.0109	0.0046	5.010E-08	2.440	50.400	2.333E-04
		0.0283	0.0046	5.010E-08	6.334	131.500	2.346E-03
Voermans et al. (2017)	S4	0.0066	0.006	3.960E-08	0.970	73.220	3.674E-05
Voermans et al. (2018)	M8	0.0060	0.01	1.100E-07	1.480	111.850	2.435E-04
	M9	0.0069	0.01	1.100E-07	1.700	128.520	4.202E-04
	L12	0.0042	0.025	6.870E-07	2.560	193.060	1.564E-04
	L13	0.0064	0.025	6.870E-07	3.900	293.980	7.692E-04
	L14	0.0081	0.025	6.870E-07	4.970	374.540	1.280E-03
	L15	0.0103	0.025	6.870E-07	6.300	475.000	2.215E-03
Present study	Base-HF	0.1683	0.01	7.500E-07	145.785	4208.443	2.257E-01
	Low Re-HF	0.0128	0.01	7.500E-07	11.071	319.602	8.243E-03
	Moderate Re-HF	0.0736	0.01	7.500E-07	63.735	1839.877	9.538E-02
	High Re-HF	2.0055	0.01	7.500E-07	1736.825	50137.814	2.677E+00
	Compact-HF	0.1311	0.01	9.877E-08	41.186	3276.291	2.085E-01
	Shallow-HF	0.3450	0.01	7.500E-07	298.778	8624.991	3.541E-01
	Deep-HF	0.0970	0.01	7.500E-07	84.038	2425.964	7.657E-02
	Base-IF	0.0931	0.01	N/A	N/A	2326.839	8.319E-02
	Low Re-IF	0.0077	0.01	N/A	N/A	192.061	2.661E-03
	Moderate Re-IF	0.0448	0.01	N/A	N/A	1119.012	2.585E-02
	High Re-IF	1.0359	0.01	N/A	N/A	25896.828	9.697E-01
	Compact-IF	0.0994	0.01	N/A	N/A	2485.128	1.492E-01

	Shallow-IF	0.1226	0.01	N/A	N/A	3063.981	5.639E-02
	Deep-IF	0.0690	0.01	N/A	N/A	1724.241	3.470E-02

References

Bear, J. (1972). *Dynamics of fluids in porous media.* Elsevier, New York.

Elliott, A. H., & Brooks, N. H. (1997). Transfer of nonsorbing solutes to a streambed with bed forms: Laboratory experiments. *Water Resources Research*, *33*(1), 137–151.

Engelund, F. (1970). Instability of erodible beds. *Journal of Fluid Mechanics*, *42*(2), 225–244.

Garcia, M. (2008). *Sedimentation engineering: processes, measurements, modeling, and practice. asce manuals and reports on engineering practice no. 110. a.* American Society of Civil Engineers. Reston, VA.

Grant, S. B., Stewardson, M. J., & Marusic, I. (2012). Effective diffusivity and mass flux across the sediment-water interface in streams. *Water Resources Research*, *48*(5).

Han, X., Fang, H., He, G., & Reible, D. (2018). Effects of roughness and permeability on solute transfer at the sediment water interface. *Water research*, *129*, 39–50.

Lian, Y. P., Dallmann, J., Sonin, B., Roche, K. R., Packman, A. I., Liu, W. K., & Wagner, G. J. (2021). Double averaging analysis applied to a large eddy simulation of coupled turbulent overlying and porewater flow. *Water Resources Research*, *57*(11), e2021WR029918.

Manes, C., Pokrajac, D., McEwan, I., & Nikora, V. (2009). Turbulence structure of open channel flows over permeable and impermeable beds: A comparative study. *Physics of Fluids*, *21*(12), 125109.

Marion, A., Bellinello, M., Guymer, I., & Packman, A. (2002). Effect of bed form geometry on the penetration of nonreactive solutes into a streambed. *Water Resources Research*, *38*(10), 27–1.

Nagaoka, H., & Ohgaki, S. (1990). Mass transfer mechanism in a porous riverbed. *Water Research*, *24*(4), 417–425.

O'Connor, B. L., & Harvey, J. W. (2008). Scaling hyporheic exchange and its influence on biogeochemical reactions in aquatic ecosystems. *Water Resources Research*, *44*(12).

O'Connor, B. L., & Hondzo, M. (2008). Dissolved oxygen transfer to sediments by sweep and eject motions in aquatic environments. *Limnology and Oceanography*, *53*(2), 566–578.

O'Connor, B. L., Hondzo, M., & Harvey, J. W. (2009). Incorporating both physical and kinetic limitations in quantifying dissolved oxygen flux to aquatic sediments. *Journal of Environmental Engineering*, *135*(12), 1304–1314.

Packman, A. I., Salehin, M., & Zaramella, M. (2004). Hyporheic exchange with gravel beds: Basic hydrodynamic interactions and bedform-induced advective flows. *Journal of Hydraulic Engineering*, *130*(7), 647–656.

Steinberger, N., & Hondzo, M. (1999). Diffusional mass transfer at sediment-water interface. *Journal of environmental engineering*, *125*(2), 192–200.

Tonina, D., & Buffington, J. M. (2007). Hyporheic exchange in gravel bed rivers with pool-riffle morphology: Laboratory experiments and three-dimensional modeling. *Water Resources Research*, *43*(1).

Voermans, J. J., Ghisalberti, M., & Ivey, G. (2017). The variation of flow and turbulence across the sediment–water interface. *Journal of Fluid Mechanics*, *824*, 413–437.

Voermans, J. J., Ghisalberti, M., & Ivey, G. N. (2018). A model for mass transport across the sediment-water interface. *Water Resources Research*, *54*(4), 2799–2812.